https://doi.org/10.5194/egusphere-2024-3010
Preprint. Discussion started: 27 September 2024

Mean ocean temperature change and decomposition of the benthic $\delta^{18}O$ record over the last 4.5 Myr

Peter U. Clark[1,2]†, Jeremy D. Shakun[3]†, Yair Rosenthal[4,5], Chenyu Zhu[6], Jonathan M. Gregory[7,8], Peter Köhler[9], Zhengyu Liu[10], Daniel P. Schrag[11], Patrick J. Bartlein[12]

[1]College of Earth, Ocean, and Atmospheric Sciences, Oregon State University, Corvallis, OR 97331
[2]School of Geography and Environmental Sciences, University of Ulster, Coleraine, Northern Ireland, UK BT52 1SA
[3]Department of Earth and Environmental Sciences, Boston College, Chestnut Hill, MA 02467
[4]Department of Marine and Coastal Science, Rutgers The State University, New Brunswick, NJ 08901
[5]Department of Earth and Planetary Sciences, Rutgers The State University, New Brunswick, NJ 08901
[6]Institute of Atmospheric Physics, Chinese Academy of Sciences, Beijing, China
[7]National Center for Atmospheric Science, University of Reading, Reading, UK
[8]Met Office Hadley Centre, Exeter, UK
[9]Alfred-Wegener-Institut Helmholtz-Zentrum für Polar- und Meeresforschung, Bremerhaven, Germany
[10]Department of Geography, The Ohio State University, Columbus, OH 43210
[11]Department of Earth and Planetary Sciences, Harvard University, Cambridge, MA 02138
[12]Department of Geography, University of Oregon, Eugene, OR 97403-1251

[*]*Correspondence to:* clarkp@onid.orst.edu
†These authors contributed equally to this work.

https://doi.org/10.5194/egusphere-2024-3010
Preprint. Discussion started: 27 September 2024

Abstract. We use a recent compilation of global mean sea surface temperature changes (ΔGMSST) over the last 4.5 Myr together with independent proxy-based reconstructions of bottom water or deep ocean temperatures to infer changes in mean ocean temperature (ΔMOT). We find that the ratio of ΔMOT/ΔGMSST, which is also a measure of ocean heat storage efficiency, was around 0.5 before the Middle Pleistocene Transition (MPT, 1.5-0.9 Ma), but was 1 thereafter. This finding is also supported when using our ΔMOT to decompose a global mean benthic $\delta^{18}O$ stack into its temperature and seawater components. However, further corrections in benthic $\delta^{18}O$, probably due to a long-term diagenetic overprint, are necessary to explain reconstructed Pliocene sea level highstands. Finally, we develop a theoretical understanding of why the ocean heat storage efficiency changed over the Plio-Pleistocene. According to our conceptual model, heat uptake and temperature in the non-polar upper ocean is mainly driven by wind, while changes in the deeper ocean in both polar and non-polar waters occur due to high-latitude deepwater formation. We propose that deepwater formation was substantially reduced prior to the MPT, effectively decreasing ΔMOT with respect to ΔGMSST. We attribute these changes in deepwater formation across the MPT to long-term cooling which caused a change starting ~1.5 Ma from a highly stratified Southern Ocean due to warm SSTs and reduced sea-ice extent to a Southern Ocean which, due to colder SSTs and increased sea-ice extent, had a greater vertical exchange of water masses.

https://doi.org/10.5194/egusphere-2024-3010
Preprint. Discussion started: 27 September 2024

1 Introduction

Changes in ocean heat storage play an important role in mitigating the Earth's surface temperature response to a radiative forcing (Gregory et al., 2002) and also influence sea-level change (Church et al., 2013) and ocean stratification, with the latter affecting the rate of ocean heat uptake (Newsom et al., 2023), the efficiency of the oceanic carbon sink (Bronselaer and Zanna, 2020), and large-scale circulation (Fox-Kemper et al., 2021). Most reconstructions of changes in bottom water temperature (ΔBWT), deep-ocean temperature (ΔDOT), and mean ocean temperature (ΔMOT)[1] relative to pre-Industrial (PI) are in good agreement in showing orbital-scale variations of ~2.5°C to 3.5°C over the last ~0.7 Myr (Sosdian and Rosenthal, 2009; Elderfield et al., 2012; Shakun et al., 2015; Haeberli et al., 2021; Shackleton et al., 2023; Martin et al., 2002) (see Section 2). Reconstructions of ΔBWT and ΔDOT that span the last 4.5 Myr also agree in showing a long-term cooling over much of this interval, but differ by as much as 2.5°C during the Pliocene (Fig. 1) (Bates et al., 2014; Hansen et al., 2013; Lear et al., 2003; Rohling et al., 2021; Cramer et al., 2011; De Boer et al., 2014; Rohling et al., 2022; Westerhold et al., 2020; Evans et al., 2024). Differences among the reconstructions on both of these timescales may reflect some combination of (1) differences in the calibration of Mg/Ca-based reconstructions as well as in the process of accounting for changes in its seawater (sw) ratio Mg/Ca_{sw} and carbonate ion concentration (Cramer et al., 2011; Rosenthal et al., 2022), (2) proxy-based reconstructions that sample local BWT that is not representative of DOT or MOT (Lear et al., 2003; Woodard et al., 2014), (3) an unaccounted-for nonstationarity in the relationship between $\delta^{18}O_b$ and sea level that is used to derive BWT or DOT (Bates et al., 2014; Rohling et al., 2021; Rohling et al., 2022; Waelbroeck et al., 2002), and (4) scaling of a $\delta^{18}O_b$ range to an inferred DOT range (LGM-Holocene) (Hansen et al., 2013; Westerhold et al., 2020; Hansen et al., 2023) that assumes stationarity in this scaling over the last 4.5 Ma and underestimates the DOT range by ~70% (Haeberli et al., 2021; Shackleton et al., 2023).

[1] The terms "bottom water temperature," "deep-ocean temperature," and "deep-sea temperature" are commonly used interchangeably in paleoceanography to refer to depths >200 m. In some cases, these terms have been used for the temperature of a specific site (Waelbroeck et al., 2002; Sosdian and Rosenthal, 2009; Elderfield et al., 2012) or for the entire ocean >200 m (Hansen et al., 2013; Rohling et al., 2022). The latter meaning is not equivalent to "mean ocean temperature" (MOT) since that includes the surface ocean, but the small volume of this surface layer means that the global ocean temperature >200 m will be comparable to MOT. Finally, these terms do not distinguish between water depths that are commonly used to describe processes and patterns of ocean heat storage: sea surface (skin) with zero heat capacity, upper (0-700 m), intermediate (700-2000 m), deep (2000-4000m), and abyssal (>4000 m) (Purkey et al., 2019; Fox-Kemper et al., 2021; Cheng et al., 2022). Here we use the term "bottom water temperature" (BWT) for a site-specific temperature reconstruction and "deep-ocean temperature" (DOT) for temperature of the whole ocean that is >200 m. We also distinguish among the depth layers (upper, intermediate, deep, and abyssal) when discussing ocean heat storage.

https://doi.org/10.5194/egusphere-2024-3010
Preprint. Discussion started: 27 September 2024

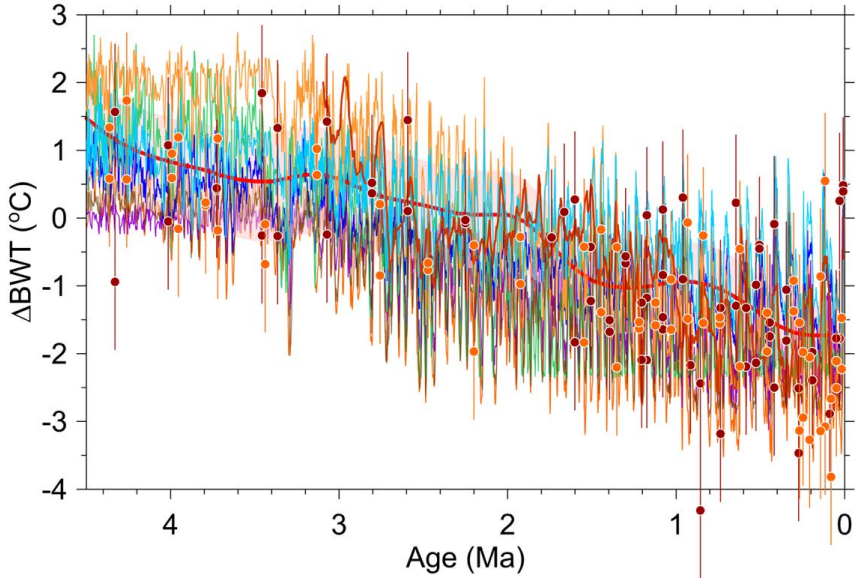

Figure 1. Reconstructions of changes in bottom water temperature (ΔBWT) since 4.5 Ma. Upper orange line is from Evans et al. (2024) referenced to pre-Industrial (PI). Purple line is from Rohling et al. (2021) referenced to PI. Dark brown line is from Rohling et al. (2022) referenced to PI. Red line with uncertainty in pink is the 2-Myr smoothed ΔBWT reconstruction from Cramer et al. (2011) using their equation 7b with 90% confidence interval. BWT's were mean shifted by 2.1°C so that they have the same long-term mean as our ΔGMOT reconstruction over the last 400 kyr. Blue line is ΔBWT reconstruction from Hansen et al. (2013). BWT's were mean shifted by 1°C so that they are referenced to the Holocene (i.e., 0°C for last 10 kyr). Green line is ΔBWT reconstruction from Bates et al. (2014). BWT's were mean shifted by 1.46°C so that they are referenced to the Holocene (i.e., 0°C for last 10 kyr). Orange line is ΔMOT reconstruction from de Boer et al. (2014) referenced to PI. Orange symbols with 1σ uncertainty is ΔBWT reconstruction from ODP site 806 (Lear et al., 2003). Mg/Ca BWT's were mean shifted by -1.73°C to fall within same range as our ΔMOT reconstruction for last 800 kyr. Red-brown symbols with 1σ uncertainty is ΔBWT reconstruction from ODP site 926 (Lear et al., 2003). Mg/Ca BWT's were mean shifted by -1.73°C so that they are referenced to the Holocene (i.e., 0°C for last 10 kyr).

Here we show that climate models (Fig. 2) and data (Fig. 2,3) from the last 0.7 Myr demonstrate that the ratio between ΔMOT and changes in global mean sea surface temperature (ΔGMSST), which Zhu et al. (2024) defined as the ocean heat storage efficiency (HSE = ΔMOT/ΔGMSST) when in equilibrium, is ~1, suggesting that we can use a new ΔGMSST reconstruction (Clark et al., 2024) to derive ΔMOT over this interval.[2] Comparison of the ΔGMSST reconstruction to existing ΔDOT reconstructions that extend beyond 0.7 Ma, however, clearly indicates that HSE was

[2] HSE can be interpreted as proportional to the effective heat capacity of the ocean for equilibrium changes, while the change in ocean heat content (in J) can be accounted for by regarding it as the (SST) * (HSE) * (the heat capacity of the ocean). Because HSE refers to equilibrium, it differs from ocean heat uptake efficiency which specifically describes transient climate states on decadal timescales during which the non-equilibrium of the ocean that causes a substantial rate of ocean heat uptake (in W m^{-2}) is large enough to affect the surface climate through its effect on the energy balance.

https://doi.org/10.5194/egusphere-2024-3010
Preprint. Discussion started: 27 September 2024

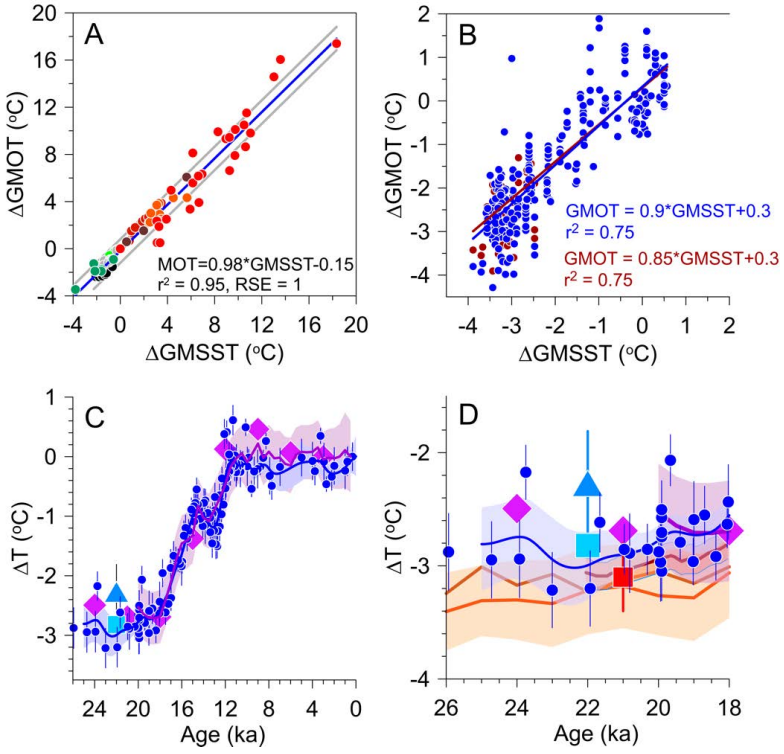

Figure 2. (**A**) Relation between equilibrium changes in global mean ocean temperature (GMOT) and global mean sea surface temperature (GMSST) from preindustrial established from 84 simulations by 30 climate models; 1σ shown by dashed blue lines. Results shown are from: model runs with CMVMc.v2 for CO_2 ≤270 ppm for no ice sheets (gray symbols) and with LGM ice sheets (black symbols) (Galbraith and De Lavergne, 2019); model runs from GENMOM for last deglaciation (green) (Alder and Hostetler, 2015); model runs from UVIC2.9 for CO_2 >420 ppm (dark brown) (Clark et al., 2016); LongRunMIP model results for CO_2 ≥2x preindustrial (PI) (orange) (Rugenstein et al., 2019); model runs for CO_2 ranging from 1x to 9x PI (red) (Goudsmit-Harzevoort et al., 2023); PMIP3 model runs for LGM boundary conditions (dark green) (Braconnot et al., 2012); and model runs with CMVMc.v2 for CO_2 >405 ppm (red brick) (Galbraith and De Lavergne, 2019). (**B**) Blue: Scatter plot of ΔGMOT derived from ice-core noble gases (Bereiter et al., 2018; Haeberli et al., 2021; Shackleton et al., 2019; Shackleton et al., 2020; Shackleton et al., 2021) versus the reconstruction of global mean sea surface temperature change from preindustrial for the last 0.7 Myr (Clark et al., 2024). Red-brown: Scatter plot of ΔGMOT derived from ice-core noble gases (Bereiter et al., 2018; Haeberli et al., 2021; Shackleton et al., 2019; Shackleton et al., 2020; Shackleton et al., 2021) with glacial maximum temperatures increased by 0.38°C (Seltzer, 2024) versus the reconstruction of global mean sea surface temperature change from preindustrial for the last 0.7 Myr (Clark et al., 2024). (**C**) Reconstructed changes in GMOT and deep-ocean temperature (DOT) since the Last Glacial Maximum relative to pre-Industrial. Blue symbols with 1σ uncertainty are GMOT derived from ice-core noble gases, with spline fit to these data with 1σ uncertainty shown by blue curve and 1σ confidence envelope (Shackleton et al., 2023). Purple diamonds from Shakun et al. (2015). Light blue square is from Rohling et al. (2022). Thick purple line and 1σ confidence envelope from Zhu et al. (2024). Light blue triangle with 1σ uncertainty is from Seltzer et al. (2024). (**D**) Reconstructed changes in GMOT, deep-ocean temperature, and global mean sea surface temperature (GMSST) during the Last Glacial Maximum. Symbols for GMOT and DOT same as in (**C**). Red square with 1σ uncertainty is GMSST from Tierney et al. (2020). Dark red line and 1σ confidence envelope from Shakun et al. (2012). Red brown line from Friedrich and Timmermann (2020). Orange line and 1σ confidence envelope from Clark et al. (2024).

smaller than 1 prior to 1.5 Ma (Fig. 4). We constrain the decrease in HSE back to 4.5 Myr by scaling ΔGMSSTs against several ΔBWT reconstructions that closely approximate ΔDOT. Decomposing the benthic $\delta^{18}O$ record ($\delta^{18}O_b$) into its temperature ($\delta^{18}O_T$) and seawater ($\delta^{18}O_{sw}$) components provides independent support for a decrease in HSE

https://doi.org/10.5194/egusphere-2024-3010
Preprint. Discussion started: 27 September 2024

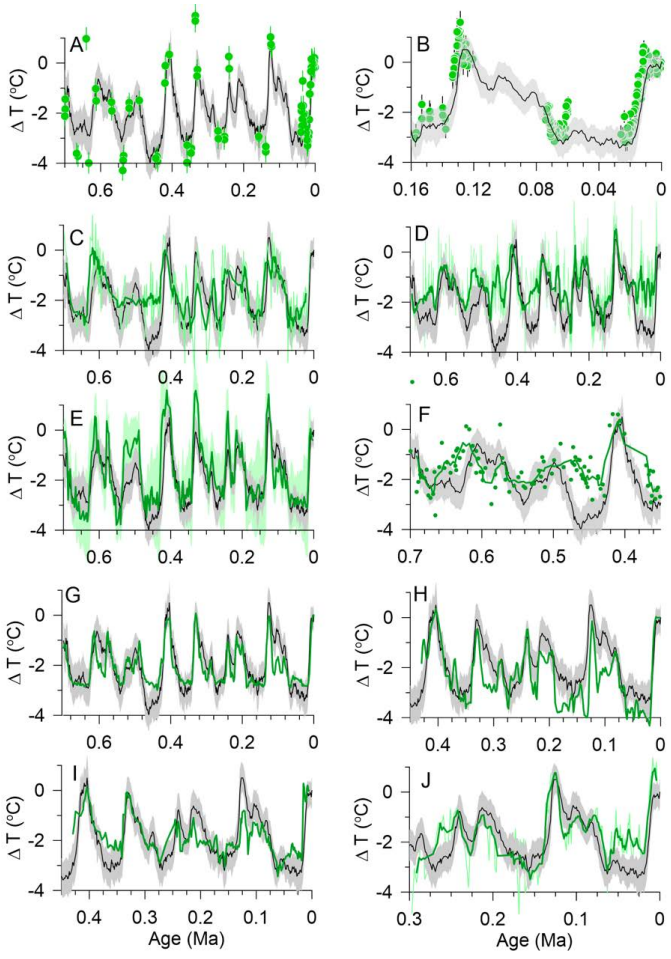

Figure 3. Comparison of the reconstruction of global mean sea surface temperature change from preindustrial (Clark et al., 2024) (black) to proxy reconstructions of bottom water temperature anomalies (ΔBWT) and ΔGMOT (green). (**A**) ΔGMOT reconstruction from Haeberli et al. (2021). (**B**) ΔGMOT reconstructions from Shackleton et al. (2020), Shackleton et al. (2021), and Shackleton et al. (2023). (**C**) Mg/Ca-based ΔBWT reconstruction from Sosdian and Rosenthal (2009) (5-pt running average shown by dark green line). (**D**) Mg/Ca-based ΔBWT reconstruction from Elderfield et al. (2012) (11-pt running average shown by dark green line). (**E**) ΔBWT reconstruction from Shakun et al. (2015). (**F**) Mg/Ca-based ΔBWT reconstruction from ODP site 1208 from Ford and Raymo (2020) (5-pt running average shown by green line). (**G**) ΔBWT reconstruction from Rohling et al. (2022). (**H**) ΔBWT reconstruction from ODP site 980 from Waelbroeck et al. (2002). (**I**) ΔBWT reconstruction from site 94-10 from Waelbroeck et al. (2002). (**J**) Mg/Ca-based ΔBWT reconstruction from Martin et al. (2002) (5-pt running average shown by dark green line).

<1 prior to ~1.5 Ma. We then summarize the processes that contribute to changes in ocean heat storage and mean ocean temperature which in turn provide the basis for a simple conceptual model that explains why HSE may have decreased to below 1 before 0.9 Ma.

https://doi.org/10.5194/egusphere-2024-3010
Preprint. Discussion started: 27 September 2024

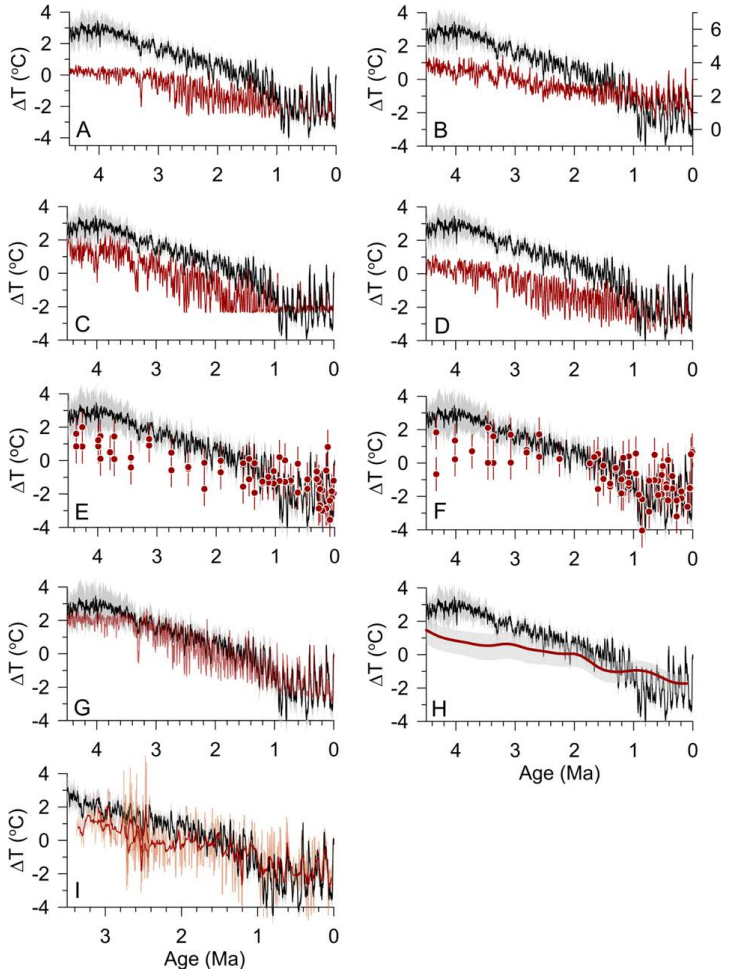

Figure 4. The reconstruction of global mean sea surface temperature change from preindustrial (Clark et al., 2024) (black) compared to reconstructions of changes in bottom water temperature (ΔBWT, dark red). (**A**) ΔBWT reconstruction from Rohling et al. (2022) referenced to preindustrial (PI). (**B**) ΔBWT reconstruction from Hansen et al. (2013). BWT's were mean shifted by 1ºC so that they are referenced to the Holocene (i.e., 0ºC for last 10 kyr). (**C**) ΔBWT reconstruction from Bates et al. (2014). BWT's were mean shifted by 1.46ºC so that they are referenced to the Holocene (i.e., 0ºC for last 10 kyr). (**D**) ΔMOT reconstruction from de Boer et al. (2014) referenced to PI. (**E**) ΔBWT reconstruction from ODP site 806 (Lear et al., 2003). Mg/Ca BWT's were mean shifted by -1.73ºC to fall within same range as our ΔMOT reconstruction for last 800 kyr. (**F**) ΔBWT reconstruction from ODP site 926 (Lear et al., 2003). Mg/Ca BWT's were mean shifted by -1.73ºC so that they are referenced to the Holocene (i.e., 0ºC for last 10 kyr). (**G**) Deep-ocean temperature reconstruction from Evans et al. (2024) which is the Rohling et al. (2022) reconstruction (panel **A**) with pH-corrected benthic $\delta^{18}O$, referenced to PI. (**H**) 2-Myr smoothed ΔBWT reconstruction from Cramer et al. (2011) using their equation 7b with 90% confidence interval. BWT's were mean shifted by 2.1ºC so that they have the same long-term mean as our ΔMOT reconstruction over the last 400 kyr. (**I**) ΔBWT from North Atlantic DSDP site 607 for >2.9 Ma (Dwyer and Chandler, 2009) and <2.8 Ma (Sosdian and Rosenthal, 2009) (11-pt running average in dark red) and ΔBWT from North Atlantic IODP site U1313 for 2.4-2.75 Ma (Jakob et al., 2020). Site 607 data are mean shifted by -1.73ºC so that they are referenced to the early Holocene (i.e., 0ºC at 10 ka). Site U1313 data are referenced to modern BWT derived by Mg/Ca measurements on core-top samples.

https://doi.org/10.5194/egusphere-2024-3010
Preprint. Discussion started: 27 September 2024

2 Derivation of global mean ocean temperature change

2.1 Methods for bottom water temperature reconstructions

Given the uncertainties and differing assumptions used in ΔDOT reconstructions derived from $\delta^{18}O_b$ records (Bates et al., 2014; Rohling et al., 2021; Hansen et al., 2013; Westerhold et al., 2020; Rohling et al., 2022; Hansen et al., 2023; Evans et al., 2024), we use several Mg/Ca-based ΔBWT reconstructions that extend into the early Pleistocene and the Pliocene as the most direct means to assess changes in HSE. These include two low-resolution ΔBWT reconstructions, one from the equatorial Pacific (ODP site 806, 2500 m) (Fig. 4E) that samples Pacific Deep Water and one from the equatorial Atlantic (ODP site 926, 3500 m) that today is in the mixing zone between North Atlantic Deep Water (NADW) and Antarctic Bottom Water (AABW) (Lear et al., 2003) (Fig. 4F). For these two sites, we use the original Mg/Ca data from Lear et al. (2003) and the recent calibrations for *C. wuellerstorfi* (Mg/Ca=1.043Exp(0.118BWT)) and *O. umbonatus* (Mg/Ca= 1.317Exp(0.102BWT)) published by Barrientos et al. (2018). We note that temperature estimates derived from *O. umbonatus* using the new exponential calibration are consistent with those calculated using the calibration of Rathmann et al. (2004).

We also use high-resolution Mg/Ca-based ΔBWT reconstructions from DSDP site 607 (3427 m) (Dwyer and Chandler, 2009; Sosdian and Rosenthal, 2009) and nearby IODP U1313 (3426 m) (Jakob et al., 2020) in the North Atlantic (Fig. 4G). We use the original published ΔBWT reconstruction from site 607 measured on ostracodes by Dwyer and Chandler (2009). The original Mg/Ca-based ΔBWT record from site 607 (Sosdian and Rosenthal, 2009) includes measurements on the benthic species *C. wuellerstorfi* and *O. umbonatus* using the published calibration Mg/Ca= 0.15*T+1.16, which we update with the exponential calibration of Barrientos et al. (2018). Since the original record is arguably overprinted by the carbonate ion (ΔCO_3^{2-}) effect (Yu and Broecker, 2010), we have added Mg/Ca measurements of *Uvigerina sp.* (Sosdian and Rosenthal, 2010; Ford et al., 2016), an infaunal benthic foraminifera which has been shown to be insensitive to ΔCO_3^{2-} effects (Elderfield et al., 2010; Elderfield et al., 2012). We calculate *Uvigerina sp.* BWTs using the Elderfield et al. (2012) calibration (Mg/Ca=0.1*T+0.94). BWTs from site U1313 (Jakob et al., 2020) were recalculated using the Barrientos et al. (2018) calibration. The new compilation presented here, including new Mg/Ca data from *Uvigerina sp.,* demonstrates that the long-term trends are similar for all three species both in the raw Mg/Ca data and estimated BWTs, lending support to the published BWT records (Ford et al., 2016; Sosdian and Rosenthal, 2009). BWTs from site U1313 (Jakob et al., 2020) are based on *O. umbonatus* Mg/Ca and have been also recalculated using the calibration from Barrientos et al. (2018).

https://doi.org/10.5194/egusphere-2024-3010
Preprint. Discussion started: 27 September 2024

When reconstructing long-term temperature changes (>1 Ma) from Mg/Ca, it is necessary to account for variations in the seawater Mg/Ca concentration ratio. For the Mg/Ca data from the sites listed above, we follow the correction proposed by Evans and Müller (2012) relating the Mg/Ca of the calcareous shells to the Mg/Ca ratio of seawater through a power equation, where we use the seawater Mg/Ca record from Rosenthal et al. (2022) to correct measured foraminiferal Mg/Ca:

$$(Mg/Ca)_{corr} = (Mg/Ca)_{foram} * (5.3/(Mg/Ca)_{sw})^{H}$$

where $(Mg/Ca)_{sw}$ is the seawater ratio at the studied time, 5.3 is the modern seawater Mg/Ca ratio, and H is the species-specific power coefficient. We apply the $(Mg/Ca)_{corr}$ to the calibrations for benthic foraminifera and a power coefficient H=0.1 to correct for seawater changes in Mg/Ca, although choosing values anywhere between 0 and 0.4 would have a negligible effect on Pleistocene BWT. The correction for changes in seawater Mg/Ca for the benthic compilations is only about +1°C. We note that the choice of seawater Mg/Ca or the calibration equation has minimal effect on the temperature reconstructions for the past 5 Myr (Meinicke et al., 2021; Rosenthal et al., 2022).

We also use a smoothed BWT reconstruction based on a compilation of Mg/Ca records derived from six species or genera of benthic foraminifera (Cramer et al., 2011) (Fig. 4H). Because *O. umbonatus* is present throughout the study interval (0-60 Ma), Cramer et al. (2011) inferred Mg/Ca offsets between *O. umbonatus* and the other taxa and then applied two published Mg/Ca calibrations derived from core-top *O. umbonatus* to the entire data set (their equations 7a and 7b). It is not clear why the calibrations differ, but they lead to significant differences in the estimated amount and rate of cooling over the last 10 Myr. We here use the equation 7b reconstruction in Cramer et al. (2011) based on Rathmann et al. (2004), since it is supported by the newer calibration of Barrientos et al. (2018). Although the smoothed reconstruction is based on Mg/Ca data from eight different sites, it is largely based on data from sites 806 and 926 for the last 4.5 Myr.

2.2 Mean ocean temperature since 0.7 Ma

Allowing for a 10^3-yr ocean response time (Rugenstein et al., 2019; Rugenstein et al., 2016; Li et al., 2013), many climate model simulations run to equilibrium under a variety of constant forcings relative to present day show an HSE of ~1 ($\Delta MOT = 0.98*\Delta GMSST-0.15$, 1σ of the residuals = 1°C, $R^2 = 0.95$, n = 84) (Fig. 2A). We assess this model relationship by comparing a ΔGMSST reconstruction (Clark et al., 2024) with low-resolution Antarctic ice-core noble-gas records of ΔMOT for the last 0.7 Myr (Haeberli et al., 2021; Shackleton et al., 2023). The good

https://doi.org/10.5194/egusphere-2024-3010
Preprint. Discussion started: 27 September 2024

agreement (R^2 = 0.75) between ice-core ΔMOT and ΔGMSST suggests an HSE of ~0.9 which, within uncertainties, agrees with an HSE of ~1 found in models run to equilibrium (Fig. 2B, 3A, 3B).

The temporal change in ΔBWT and ΔGMSST reconstructions also largely agree (Fig. 3), with dominant orbital-scale variability, although there is one exception in the ODP site 1123 reconstruction (Fig. 3D) (Elderfield et al., 2012) when ΔBWT approaches interglacial levels during MIS12 (~0.45 Ma), in contrast to the cold temperatures in the ΔGMSST and ΔMOT reconstructions (Fig. 3A) (Haeberli et al., 2021). Several ΔBWT reconstructions differ from the ΔGMSST reconstruction in the amplitude of change, particularly during glacial periods (Fig. 3C, 3D, 3H), which we attribute to site-specific ΔBWT records not necessarily sampling the three-dimensional temperature structure of the ocean that gives rise to ΔMOT. Calibration uncertainties for the Mg/Ca records and changes in carbonate saturation, which are greatest at low temperatures, may also play a role. Despite these differences, the general agreement between the ΔGMSST reconstruction and Mg/Ca-based ΔBWT reconstructions further supports an HSE~1 over the last 0.7 Myr.

Multiple reconstructions of ΔGMSST and ΔMOT that span the Last Glacial Maximum (LGM, 26-18 ka) provide further constraints on HSE at that time (Fig. 2C, 2D). There is good agreement among ΔGMSST reconstructions (referenced to PI), with proxy-based estimates of -3.0±0.1ºC (18-22 ka average) (Shakun et al., 2012), –2.9°C (–3.0° to –2.7°C, 95% confidence interval (CI) (23-19 ka average) (Tierney et al., 2020), and -3.3±0.4ºC (26-18 ka average) (Clark et al., 2024), and an estimate from a global climate model with data assimilation of –3.1°C (–3.4° to –2.9°C, 95% CI) (23-19 ka average) (Tierney et al., 2020), with an average LGM ΔGMSST of -3.0±0.2ºC.

There is also good agreement among existing ΔMOT and ΔDOT reconstructions (referenced to PI) for the LGM (Fig. 2C, 2D). We note that the ΔDOT reconstructions by Hansen et al. (2013; 2023) are based on an inferred LGM cooling of –2° and are thus not considered here. Shakun et al. (2015) found an LGM average cooling of -2.63°C and Rohling et al. (2022) (updated from Rohling et al. (2021)) reconstructed an LGM average cooling of -2.82±0.17°C. Shackleton et al. (2023) standardized previously published ice-core noble gas ΔMOT reconstructions (Bereiter et al., 2018; Baggenstos et al., 2019; Shackleton et al., 2019; Shackleton et al., 2020) and reported a data-based LGM average ΔMOT of -2.76±0.27°C and a spline average of -2.83±0.5°C. We also note that a ΔDOT reconstruction for 0-20 ka derived by subtracting global $\delta^{18}O_{sw}$ from $\delta^{18}O_b$ records (Zhu et al., 2024) is in good agreement with the spline ΔMOT reconstruction (Shackleton et al., 2023), including during the period of LGM overlap (18-20 ka) (Fig. 2C, 2D). Taking

https://doi.org/10.5194/egusphere-2024-3010
Preprint. Discussion started: 27 September 2024

the average LGM ΔMOT (-2.76±0.31ºC) with the average LGM ΔGMSST (-3.0±0.2ºC) suggests an LGM HSE of 0.92, or the same as when using the ice-core noble gas ΔMOT reconstructions for the last 0.7 Myr (Fig. 2B) and, within uncertainty, with an HSE of ~1 suggested by models (Fig. 2A).

Recent work, however, has argued that changes in noble-gas saturation states of the deep ocean during the LGM may have resulted in a cold bias in the ice-core data equivalent to -0.38±0.37ºC (Seltzer, 2024) to -0.50 ±0.67ºC (Pöppelmeier et al., 2023). Despite these similar results, Seltzer et al. (2024) noted that Pöppelmeier et al. (2023) were unable to reconcile their result from simulated air-sea gas exchange with the ice-core data and thus based their MOT cooling on a climate model. The cold bias identified by Seltzer et al. (2024) is based on an ensemble of five PMIP3 climate models that suggest air-sea disequilibria due to stronger high-latitude winds, from which they argued that LGM ΔMOT was -2.27±0.46ºC, corresponding to an LGM HSE of ~0.8 when using an average LGM ΔGMSST of -3.0±0.2ºC. Seltzer et al. (2024) did not elaborate on how this effect may have differed at other times, but we can assume that high-latitude winds would have weakened from their LGM maxima, resulting in a diminished effect on air-sea disequilibria at those times. As a first-order approximation of how this would be expressed during other glacial maxima, we decreased all glacial maxima ΔMOT's in the 0.7-Myr ice-core noble gas reconstruction (Haeberli et al., 2021) by 0.38ºC, resulting in a decrease of HSE from 0.9 to 0.85 (Fig. 2B).

We thus conclude that the potential LGM cold bias in ΔMOT does not substantially change the evidence that HSE was ~1 within the uncertainties of the data. At the same time, Seltzer et al. (2024) recognized that current understanding of changes in LGM high-latitude wind speed (and thus air-sea disequilibria) in both observations and models is highly uncertain. For example, more-recent modeling suggests that high-latitude Southern Hemisphere wind speeds during the LGM weakened by 15% (Zhu et al., 2021) to 25% (Gray et al., 2023) as opposed to the 11±23% increase in the PMIP3 model average (largely driven by one model). As Seltzer et al. (2024) note, "Future improvements in our understanding of high-latitude winds in the LGM will help to substantially reduce uncertainties in LGM MOT." In the meantime, the good agreement between independent estimates of ΔDOT from marine proxy records (Shakun et al., 2015; Rohling et al., 2022; Zhu et al., 2024) with the ice-core ΔMOT estimate that neglects air-sea disequilibrium (Shackleton et al., 2023) (Fig. 2C) suggests a negligible effect of air-sea disequilibrium on the ice-core data.

https://doi.org/10.5194/egusphere-2024-3010
Preprint. Discussion started: 27 September 2024

2.3 Pliocene and early Pleistocene mean ocean temperature

All ΔBWT and ΔDOT reconstructions that extend beyond 0.7 Ma suggest that HSE was smaller than 1 before 1.5 Ma, with these temperature anomalies being 1-3°C less than ΔGMSST during the Pliocene (Fig. 4). As discussed further in section 4, temperature change of the ocean interior in response to surface forcing is nonuniform, with warming of the upper half of the ocean being stronger than GMSST warming as opposed to weaker in the lower half of the ocean (Bronselaer and Zanna, 2020; Fox-Kemper et al., 2021; Rugenstein et al., 2016; Zhu et al., 2024). To assess the relationship of ΔBWT at the Pacific and Atlantic core sites to ΔGMOT, we use results from the Transient Climate Evolution (iTRACE) simulation performed with the isotope-enabled Community Earth System Model version 1.3 that has reproduced the observed evolution of global climate and water masses from 21 ka to the early Holocene (11 ka) (Gu et al., 2020; He et al., 2021). The simulation is forced by changes in solar insolation from orbital changes (ORB), greenhouse gases (GHGs), reconstructed ice sheets (ICE), and meltwater fluxes (MWF), with the latter causing millennial-scale variations in ocean heat storage and MOT through its effect on the Atlantic meridional overturning circulation (AMOC) (Zhu et al., 2024).

Given that the Pacific Ocean constitutes ~50% of the total ocean volume, Lear et al. (2003) considered site 806 BWT to closely represent MOT. This inference is consistent with iTRACE ΔBWTs at the location of site 806 that closely parallel ΔMOT throughout the simulation (Fig. 5A). In this regard, we note that the Cramer et al. (2011) reconstruction, being largely weighted by site 806 data for the 1-4.5 Ma interval but with a different calibration than used in Lear et al. (2003), also represents a close approximation of ΔMOT. On the other hand, sites 926, 607, and U1313 were largely bathed by NADW prior to ~1.5 Ma after which NADW shoaled and was replaced by AABW at these sites during glaciations (Lisiecki, 2014). In both cases, the associated water masses account for a significantly smaller fraction of total ocean volume and their BWTs may thus not reflect MOT. Despite being under a greater influence of millennial-scale changes in the Atlantic meridional overturning circulation (AMOC), simulated ΔBWTs at Atlantic sites 926 and 607 warm as much as MOT by 11 ka (Fig. 5A). These similar changes in ΔBWT are further shown when combining the ΔBWT data from sites 806 and 926 (Lear et al., 2003), the smoothed ΔBWT reconstruction from Cramer et al. (2011) (comprised largely of data from sites 806 and 926), and the ΔBWT data from sites 607 (Dwyer and Chandler, 2009; Sosdian and Rosenthal, 2009) and U1313 (Jakob et al., 2020) (Fig. 5B). These results

https://doi.org/10.5194/egusphere-2024-3010
Preprint. Discussion started: 27 September 2024

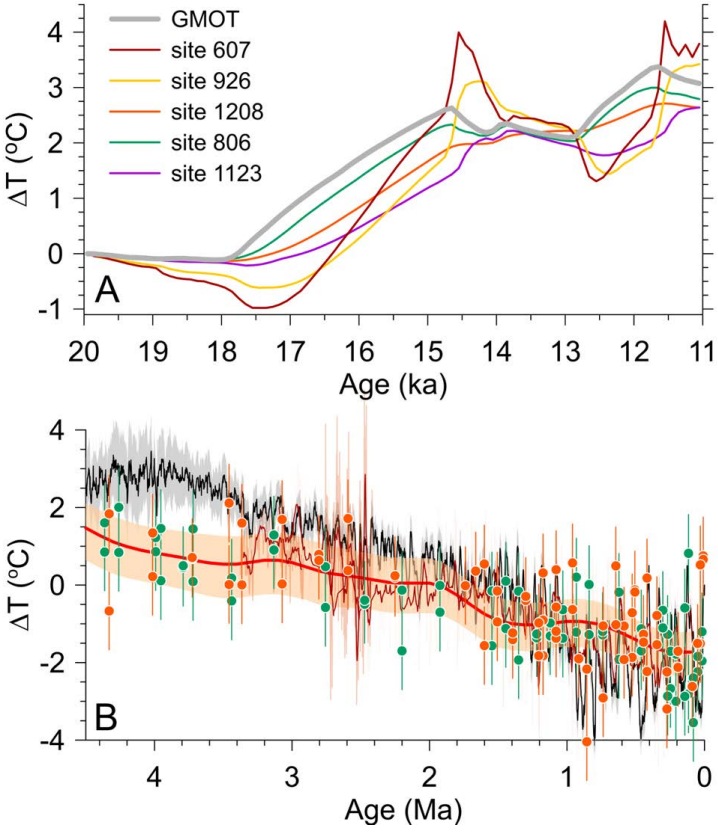

Figure 5. (**A**) Simulated changes in global mean ocean temperature (GMOT) relative to 20 ka from the iTRACE experiment as well as for five sites with ΔBWT reconstructions (Zhu et al., 2024). (**B**) Global mean sea surface temperature change (black line, 1σ uncertainty) compared to Mg/Ca-based ΔBWT reconstructions from Pacific ODP site 806 (green circles) (Lear et al., 2003), North Atlantic ODP site 926 (orange circles) (Lear et al., 2003), North Atlantic sites 607 for >2.9 Ma (Dwyer and Chandler, 2009) and <2.8 Ma (Sosdian and Rosenthal, 2009) and site U1313 for 2.4-2.75 Ma (Jakob et al., 2020) (9-, 11-, and 21-pt running averages, respectively, in dark red), and smoothed reconstruction from Cramer et al. (2011) using their equation 7b with 90% confidence interval.

thus suggest that ΔBWTs at the Pacific and Atlantic sites agree and are thus closely monitoring ΔMOT, suggesting that we can combine their ΔBWT reconstructions to approximate ΔMOT.

2.4 Testing different ocean heat storage efficiencies

To assess which HSE best agrees with the data before 1.5 Ma, we next compare in one case the combined ΔBWT data from sites 806, 926, and 607 and in another case the smoothed reconstruction from Cramer et al. (2011) (based on sites 806 and 926 with a different calibration) to three different scenarios of ΔMOT derived from our ΔGMSST reconstruction based on HSEs of 1, 0.5, and 0.1 (Fig. 6). The uncertainty on the ΔMOT-scenario reconstructions is calculated as the square root of the sum of squares of the uncertainty in the ΔGMSST reconstruction

https://doi.org/10.5194/egusphere-2024-3010
Preprint. Discussion started: 27 September 2024

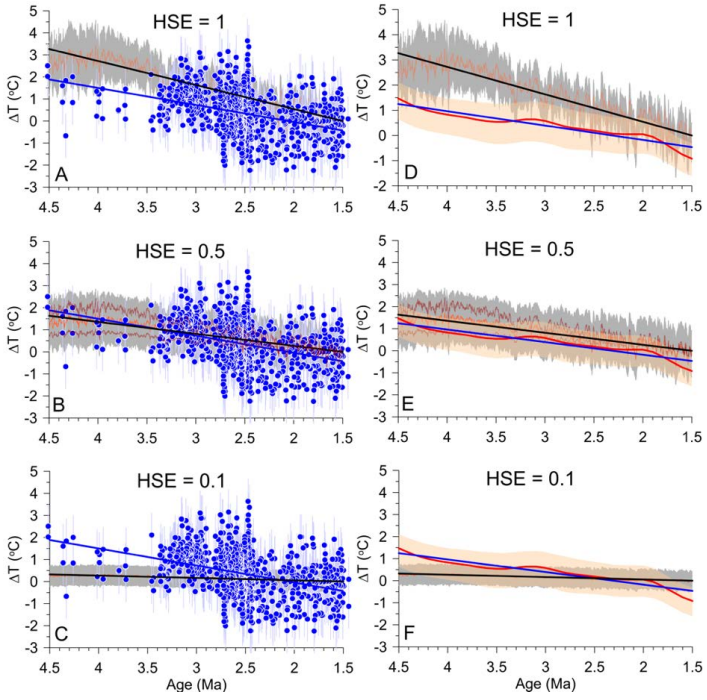

Figure 6. A-C. Our reconstructed global mean ocean temperature anomaly (ΔGMOT) for 1.5-4.5 Ma based on three different HSEs (orange lines) compared to proxy-based (Mg/Ca) reconstructions of bottom water temperature anomalies (blue) (1ºC uncertainty) (Sosdian and Rosenthal, 2009; Lear et al., 2003). 1σ uncertainty on ΔMOT reconstructions (gray fill) derived by combining in quadrature 1σ uncertainties on our ΔSST reconstruction and on the relationship between ΔGMSST and ΔGMOT (Fig. 2A). Regression lines plotted through ΔGMOT reconstructions (black) and Mg/Ca data (blue). (**A**) Our reconstructed ΔGMOT based on HSE = 1. (**B**) Our reconstructed ΔGMOT based on HSE = 0.5. Also shown are ΔGMOT reconstructions based on HSE = 0.7 and HSE = 0.3 (brown lines), which closely encompass the 1σ uncertainty on our ΔGMOT reconstruction based on HSE = 0.5. (**C**) Our reconstructed ΔGMOT based on HSE = 0.1 (falls under the corresponding regression line). The decrease in uncertainties on our ΔGMOT reconstructions reflects the decrease in uncertainty on our scaled ΔGMSST reconstructions. **D-F**. Our reconstructed global mean ocean temperature anomaly (ΔGMOT) for 1.5-4.5 Ma based on three different HSEs (orange lines) compared to 2-Myr smoothed ΔBWT reconstruction from Cramer et al. (2011) using their equation 7b (red line) with 90% confidence interval (orange shading). Their BWT's were mean shifted by 2.1ºC so that they have the same long-term mean as our ΔGMOT reconstruction over the last 400 kyr. (**D**) Our reconstructed ΔGMOT based on HSE = 1. (**E**) Our reconstructed ΔGMOT based on HSE = 0.5. Also shown are ΔGMOT reconstructions based on HSE = 0.7 and HSE = 0.3 (brown lines), which closely encompass the 1σ uncertainty on our ΔGMOT reconstruction based on HSE = 0.5. (**F**) Our reconstructed ΔGMOT based on HSE = 0.1 (falls under the corresponding regression line).

and in the HSE derived from models (Fig. 2A). We attribute the total spread in the Mg/Ca data around its long-term trend to some combination of climate variability, analytical and calibration errors, and site location.

We find that the best agreement with the Mg/Ca-based ΔBWT data is for an HSE of ~0.5, with long-term rates of cooling between 1.5-4.5 Ma in both the data and our corresponding ΔMOT reconstruction being 0.6-0.8ºC Myr^{-1} (Fig. 6B, 6E, 7). HSE values of 0.7 and 0.3 closely encompass the uncertainty on our ΔMOT reconstruction based on an HSE = 0.5 (Fig. 6B, 6E), suggesting an HSE of 0.5±0.2. Any further decrease in HSE would suggest

https://doi.org/10.5194/egusphere-2024-3010
Preprint. Discussion started: 27 September 2024

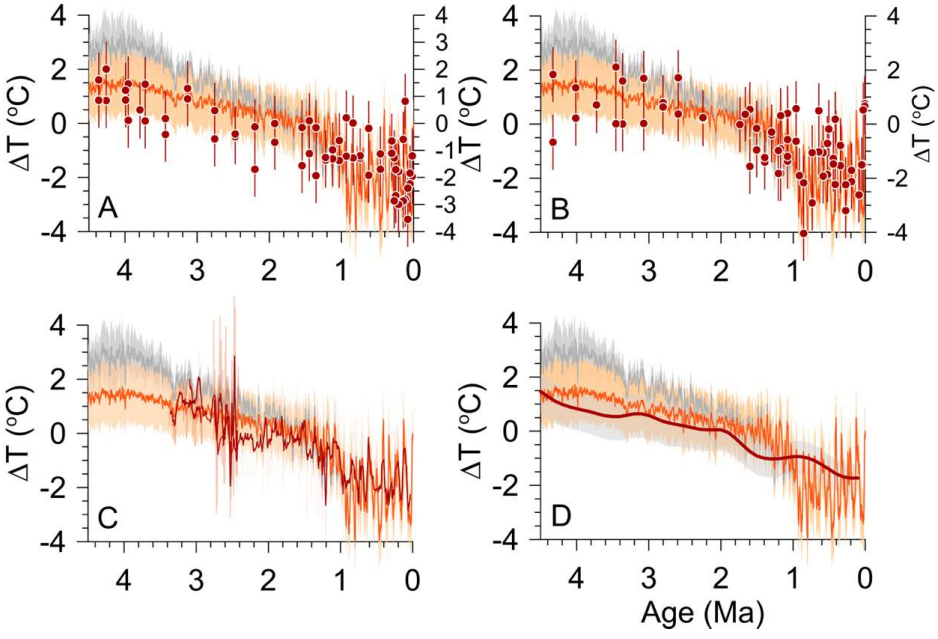

Figure 7. Our reconstructed change in mean ocean temperature (ΔGMOT) based on HSE = 0.5 before 1.5 Ma (1σ uncertainty) and HSE = 1 after 0.9 Ma with a linear increase in HSE from 0.5 to 1 between 1.5 to 0.9 Ma (orange) compared to reconstructions of bottom water temperature anomalies (ΔBWT) from Mg/Ca proxies. Also shown is ΔGMOT based on HSE = 1 (gray). (**A**) ΔBWT from equatorial Pacific ODP site 806 (Lear et al., 2003). Mg/Ca BWT's were mean shifted by -1.73°C to fall within same range as our ΔMOT reconstruction for last 800 kyr. (**B**) ΔBWT from equatorial Atlantic ODP site 926 (Lear et al., 2003). Mg/Ca BWT's were mean shifted by -1.73°C so that they are referenced to the Holocene (i.e., 0°C for last 10 kyr). (**C**) ΔBWT from North Atlantic DSDP site 607 for >2.9 Ma (Dwyer and Chandler, 2009) and <2.8 Ma (Sosdian and Rosenthal, 2009) (11-pt running average in dark red) and ΔBWT from North Atlantic IODP site U1313 for 2.4-2.75 Ma (Jakob et al., 2020). Site 607 data are mean shifted by 2.71°C so that they are referenced to the early Holocene (i.e., 0°C at 10 ka). Site U1313 data are referenced to modern BWT derived by Mg/Ca measurements on core-top sample. (**D**) Smoothed ΔBWT reconstruction from Cramer et al. (2011) (dark red line) using their equation 7b with 90% confidence interval (gray shading). BWT's were mean shifted by 2.1°C so that they have the same long-term mean as our ΔMOT reconstruction over the last 400 kyr. The 1σ uncertainty on our ΔGMOT reconstructions is derived by combining in quadrature 1σ uncertainties on the ΔGMSST reconstruction and on the relationship between ΔGMSST and ΔGMOT (Fig. 2A) which closely corresponds to a range in HSE between 0.7 and 0.3 (Fig. 6B, 6E).

virtually no change in MOT between 1.5-4.5 Ma, in contrast to the long-term cooling trend shown by all ΔBWT and ΔDOT reconstructions (Fig. 1, 4, 6B, 6E, 7).

In summary, existing constraints from Mg/Ca-based ΔBWT data and ice-core ΔMOT data show that HSE was ~1 for the last 0.7 Ma (Fig. 2B, 3) and ~0.5±0.2 for >1.5 Ma (Fig. 6). These constraints thus suggest that the increase occurred as part of the large-scale changes in ocean circulation during the middle Pleistocene transition (MPT, 0.9-1.5 Ma) (Lisiecki, 2014; Lang et al., 2016; Pena and Goldstein, 2014). Although the data do not identify the exact function by which HSE increased during this time, we make the simplifying assumption that it increased linearly from 0.5 to 1 during the MPT (Fig. 8).

https://doi.org/10.5194/egusphere-2024-3010
Preprint. Discussion started: 27 September 2024

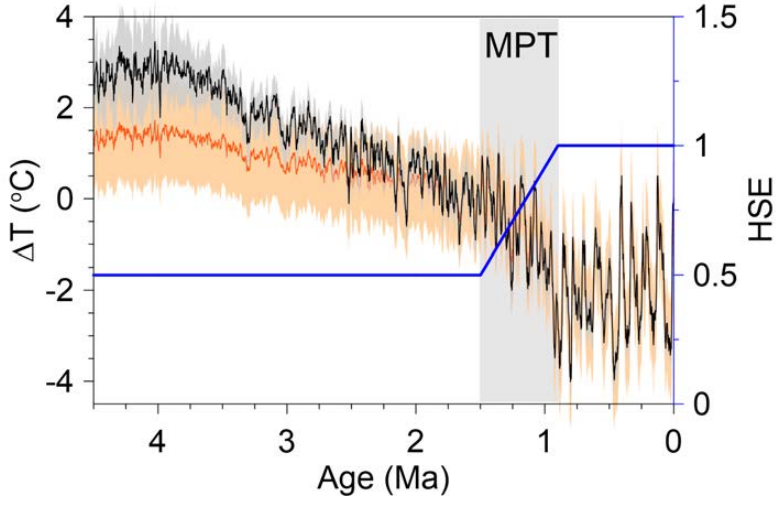

Figure 8. Our reconstructed ΔMOT (orange line) as function of ΔGMSST (black line) and HSE (blue line) that linearly increases from 0.5 to 1 across the MPT.

3 Decomposition of the benthic $\delta^{18}O$ record

3.1 Derivation of $\delta^{18}O_{sw}$ supports HSE <1 before MPT

Using our ΔMOT reconstruction to decompose the $\delta^{18}O_b$ record into its temperature ($\delta^{18}O_T$) and seawater ($\delta^{18}O_{sw}$) components provides additional support for the need to decrease HSE to <1 prior to 0.9 Ma as identified from the proxy ΔBWT data. We use the probabilistic global $\delta^{18}O_b$ stack ("Prob-stack") from Ahn et al. (2017) which, compared to the previous LR04 stack (Lisiecki and Raymo, 2005), includes a larger number of records (total = 180) that span a larger depth range of the ocean (500-4500 m) as well as uncertainties in the alignment of these records. Stacking individual $\delta^{18}O_b$ records that span such a geographic and depth range significantly increases the signal-to-noise ratio for global changes in $\delta^{18}O_b$ and its $\delta^{18}O_T$ and $\delta^{18}O_{sw}$ components while minimizing local hydrographic changes that may contribute to a single $\delta^{18}O_b$ record. We convert our ΔMOT reconstruction (Fig. 9) to $\delta^{18}O_T$ using a relation of 0.25‰ $°C^{-1}$ which is appropriate for cold deepwater temperatures (Kim and O'neil, 1997; Marchitto et al., 2014) and subtract this from the Prob-stack to derive $\delta^{18}O_{sw}$. We estimate the 1σ uncertainty on $\delta^{18}O_{sw}$ from the square root of sum of squares based on the uncertainties in our ΔMOT reconstruction, the HSE from models, and the probabilistic $\delta^{18}O_b$ stack.

Figure 9A shows that when using an HSE of 1 for the last 4.5 Myr, early Pleistocene and late Pliocene $\delta^{18}O_{sw}$ values are significantly more positive than the Mg/Ca-based reconstruction from North Atlantic site 607

https://doi.org/10.5194/egusphere-2024-3010
Preprint. Discussion started: 27 September 2024

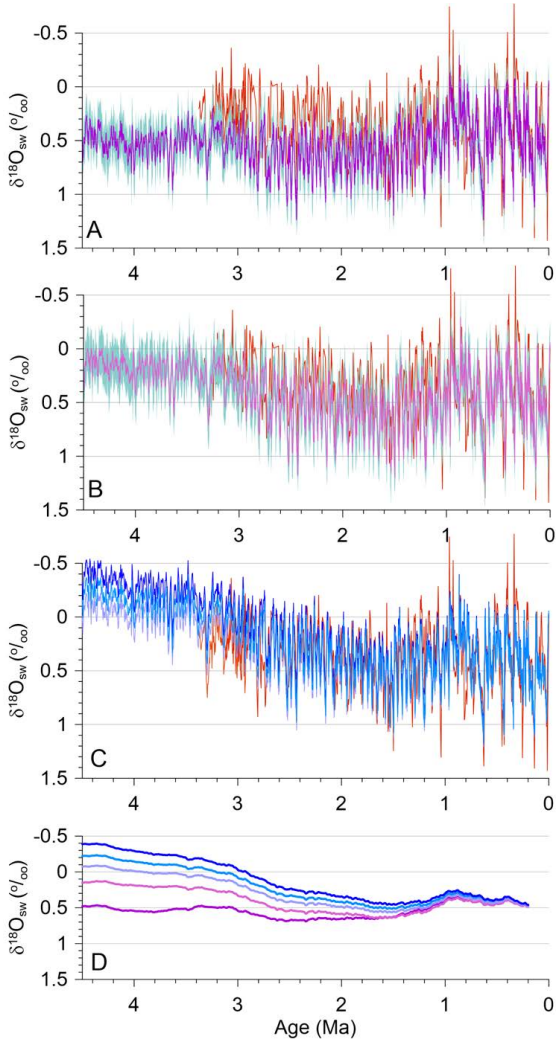

Figure 9. (**A**) Our reconstructed $\delta^{18}O$ of seawater ($\delta^{18}O_{sw}$) (1σ uncertainty) for 0-4.5 Ma based on HSE = 1 (purple) compared to proxy-based (Mg/Ca) reconstruction of $\delta^{18}O_{sw}$ (red) from North Atlantic site 607 (Sosdian and Rosenthal, 2009; Dwyer and Chandler, 2009). (**B**) Our reconstructed $\delta^{18}O$ of seawater ($\delta^{18}O_{sw}$) (1σ uncertainty) for 0-4.5 Ma based on HSE = 0.5 before 1.5 Ma (violet) compared to proxy-based (Mg/Ca) reconstruction of $\delta^{18}O_{sw}$ (red) from North Atlantic site 607 (Sosdian and Rosenthal, 2009; Dwyer and Chandler, 2009). (**C**) Our reconstructed $\delta^{18}O$ of seawater ($\delta^{18}O_{sw}$) (1σ uncertainty) for 0-4.5 Ma based on HSE = 0.5 before 1.5 Ma and removal of long-term trends of 0.05‰ Myr^{-1} ($\delta^{18}O_{sw}$-LO, light blue), 0.083‰ Myr^{-1} ($\delta^{18}O_{sw}$-INT, medium blue), and 0.12‰ Myr^{-1} ($\delta^{18}O_{sw}$-HI, dark blue) compared to proxy-based (Mg/Ca) reconstruction of $\delta^{18}O_{sw}$ (red) from North Atlantic site 607 (Sosdian and Rosenthal, 2009; Dwyer and Chandler, 2009). (**D**) Long-term running averages of the five $\delta^{18}O_{sw}$ scenarios shown in **A-C**, color coded in the same way.

(Sosdian and Rosenthal, 2009), which is the longest (0-3.2 Ma), orbitally resolved record available. This is to be expected since we used the Mg/Ca-based BWT reconstructions to constrain the reduction in HSE. However, anomalously positive $\delta^{18}O_{sw}$ values extend back to 4.5 Ma, with Pliocene interglacial values that are 0.3‰ to 0.5‰

https://doi.org/10.5194/egusphere-2024-3010
Preprint. Discussion started: 27 September 2024

more positive than average interglacial values over the last 0.8 Myr despite robust evidence for higher-than-present Pliocene sea level that require values below 0‰ (Miller et al., 2012; Raymo et al., 2018; Dumitru et al., 2019; Winnick and Caves, 2015). This suggests that too much of the $\delta^{18}O_b$ signal is being removed by the $\delta^{18}O_T$ component using an HSE of 1.

Applying our ΔMOT reconstruction (Fig. 8) results in $\delta^{18}O_{sw}$ values that are more comparable to Pliocene sea-level reconstructions, with average Pliocene interglacial $\delta^{18}O_{sw}$ values decreasing to 0‰ to -0.1‰ (Fig. 9B), thus supporting the need for the decrease in HSE prior to 1.5 Ma suggested by proxy data (Fig. 6,7). However, early Pleistocene and Pliocene $\delta^{18}O_{sw}$ values continue to be more positive than data constraints (Dwyer and Chandler, 2009; Dumitru et al., 2019; Miller et al., 2012; Jakob et al., 2020; Sosdian and Rosenthal, 2009). While a further decrease in HSE to 0.1 results in average Pliocene $\delta^{18}O_{sw}$ values of -0.2‰ (not shown) which could explain higher sea levels at that time (Raymo et al., 2018; Winnick and Caves, 2015; Dumitru et al., 2019), such a low HSE is ruled out by proxy BWT reconstructions (Fig. 6,7).

3.2 Other potential factors influencing the long-term $\delta^{18}O_b$ trend

Raymo et al. (2018) suggested that the ~0.3‰ decrease in Pliocene $\delta^{18}O_b$ values relative to late Holocene values is too small to accommodate both the higher sea levels and warmer ocean temperatures inferred for this time. They addressed this discrepency by proposing that foraminifera tests that recrystallized in pore waters that were colder than those in which they were originally buried would cause precipitation of abiotic calcite with heavier $\delta^{18}O$ values (Schrag, 1999), resulting in 3-Myr benthic foraminifera tests being ~0.25‰ heavier than tests with no diagenesis. Decreasing Pliocene $\delta^{18}O_b$ values in the Prob-stack by an additional 0.25‰ can then more readily explain the evidence for higher sea levels and warmer ocean temperatures. Applying this diagenetic process using our reconstructed MOT cooling over the past 4.5 Myr suggests that the diagenetic impact is subtle but could account for a shift of 0.2‰ to 0.4‰ over the 4.5 Myr record, with averaging of the $\delta^{18}O_b$ records in the Prob-stack integrating diagenetic effects to produce a near-constant secular change.

We cannot determine exactly how much the effect of diagenesis may have contributed to an increase in $\delta^{18}O_b$ over the least 4.5 Myr, but our assessment suggests that it is sufficient to justify a secular increase as proposed by Raymo et al. (2018). Given our assessed range, we considered three scenarios that result in a diagenetic increase in $\delta^{18}O_b$ from today of 0.15‰, 0.25‰, and 0.35‰ at 3 Ma corresponding to a long-term secular increase of 0.05‰ Myr^{-}

https://doi.org/10.5194/egusphere-2024-3010
Preprint. Discussion started: 27 September 2024

^{1} ($\delta^{18}O_{sw}$-LO), 0.083‰ Myr^{-1} ($\delta^{18}O_{sw}$-INT), and 0.12‰ Myr^{-1} ($\delta^{18}O_{sw}$-HI), respectively. In removing the secular increase for each of these scenarios from the $\delta^{18}O_b$ Prob-stack, $\delta^{18}O_{sw}$ values based on our ΔMOT reconstruction agree with reconstructed late-Pliocene and early Pleistocene $\delta^{18}O_{sw}$ values from site 607 (Fig. 9C). Although this agreement hinges on just one $\delta^{18}O_{sw}$ record that may also have experienced diagenesis, we previously showed that this site closely monitors MOT (Fig. 5). Moreover, not accounting for these combined effects (change in HSE, diagenesis) would result in long-term average $\delta^{18}O_{sw}$ values being comparable to late-Pleistocene average values throughout the last 4.5 Myr (Fig. 9D). Finally, our reconstructed long-term Pliocene $\delta^{18}O_{sw}$ values of -0.1‰ to -0.4‰ (Fig. 9D) are consistent with sea-level highstands of 20-25 m above present (Dumitru et al., 2019) even when accounting for land ice having more positive $\delta^{18}O$ values under warmer surface temperatures (Winnick and Caves, 2015), with the remaining ~0.4‰ decrease in the $\delta^{18}O_b$ record relative to the late Pleistocene consistent with the ~1.5°C ΔGMOT in our reconstruction (Fig. 8).

Another potential effect that may be comparable to diagenesis is the impact of changing carbonate ion concentration in seawater on the $\delta^{18}O$ of foraminifera shells (Spero et al., 1997). Due to higher concentrations of atmospheric CO_2 (Köhler, 2023), the 100-kyr mean carbonate ion concentration in Pliocene seawater may have been lower than during the late Pleistocene by on the order of 20 to 50 µmol kg^{-1}. Laboratory experiments (Bijma et al., 1999) and theoretical studies (Zeebe, 1999) on planktic species suggest a species-specific effect which would cause the $\delta^{18}O$ of foraminifera shells in the early Pliocene to increase by 0.1‰ to 0.3‰ relative to the late Pleistocene. Although no laboratory studies on benthic foraminifera species have been conducted, Marchitto et al. (2014) speculated that the $\delta^{18}O$ of some late-Holocene benthic species may have been influenced by pH. On the other hand, a recent study compiling 160 kyr of data from two widely abundant planktic foraminifera species in wider tropical surface waters extracted from 127 sediment cores could not confirm the carbonate ion effect as found in the laboratory (Köhler and Mulitza, 2024). Furthermore, a recent analysis of late Holocene data from the benthic foraminifera species *Cibiciddoides spp* found that only about a third of the variance in $\delta^{18}O$ can be explained by carbonate chemistry (Nederbragt, 2023). Altogether, these findings suggest that it is unlikely that the carbonate ion effect can explain the $\delta^{18}O$ corrections required to bring them in better agreement with independent deep-ocean temperature and sea-level reconstructions.

https://doi.org/10.5194/egusphere-2024-3010
Preprint. Discussion started: 27 September 2024

3.3 Temperature and $\delta^{18}O_{sw}$ controls on the Prob-stack $\delta^{18}O_b$ record

Our reconstruction shows that $\delta^{18}O_{sw}$ increased between 3.0 and 2.5 Ma in its (glacial) maxima to values that, on average, are similar to LGM values. These high glacial values in $\delta^{18}O_{sw}$ persisted throughout much of the Pleistocene (Fig. 10B). The main factor that is modulating the expression of this late Pliocene/early Pleistocene $\delta^{18}O_{sw}$

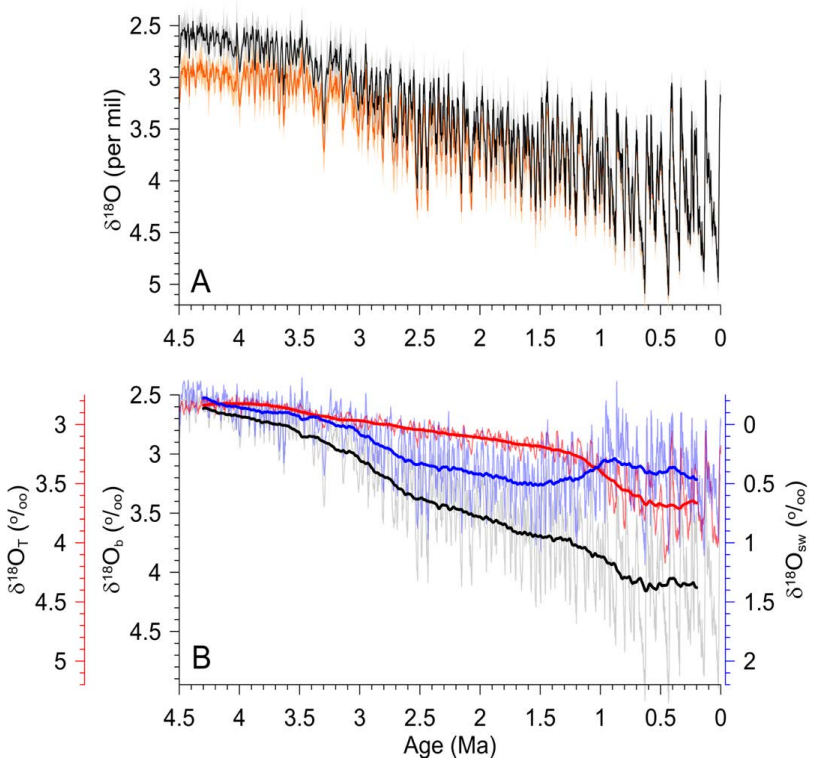

Figure 10. (**A**) Comparison of the Prob-stack $\delta^{18}O_b$ record (orange line with 1σ uncertainty) (Ahn et al., 2017) to the Prob-stack $\delta^{18}O_b$ record with the removal of a long-term secular increase of 0.083‰ Myr^{-1} (black line with 1σ uncertainty). (**B**) Comparison of the Prob-stack $\delta^{18}O_b$ record (Ahn et al., 2017) with the removal of a long-term secular increase of 0.083‰ Myr^{-1} (gray with 251-point running average in black) to our $\delta^{18}O_T$ reconstruction (light red with 251-point running average in red) and our $\delta^{18}O_{sw}$-INT reconstruction (light blue with 251-point running average in blue).

increase in the Prob-stack $\delta^{18}O_b$ is the gradual decrease in long-term average MOT (and thus increase in $\delta^{18}O_T$) relative to the increase in the rate of change in long-term average $\delta^{18}O_b$ values between 3.0-2.5 Ma (Fig. 10B). In other words, since $\delta^{18}O_T$ is only decreasing gradually, the relatively rapid increase in $\delta^{18}O_b$ between 3.0-2.5 Ma must be due to a substantial increase in $\delta^{18}O_{sw}$. After 2.5 Ma, both average $\delta^{18}O_T$ and $\delta^{18}O_{sw}$ values increase at similar rates until the onset of the MPT at 1.5 Ma. The second rapid increase in $\delta^{18}O_b$ during the MPT would then be due to the rapid decrease in $\delta^{18}O_T$, in this case resulting in a slight decrease in average $\delta^{18}O_{sw}$ values (Fig. 10B). A subsequent paper

https://doi.org/10.5194/egusphere-2024-3010
Preprint. Discussion started: 27 September 2024

will use our $\delta^{18}O_{sw}$-LO, -INT, and -HI reconstructions to derive sea level over the last 4.5 Myr that accounts for land ice having more positive $\delta^{18}O$ values under warmer surface temperatures (Winnick and Caves, 2015; Gasson et al., 2016).

3.4 Assessment of our $\delta^{18}O_{sw}$-INT reconstruction

We assess our $\delta^{18}O_{sw}$-INT reconstruction by comparing them with other $\delta^{18}O_{sw}$ reconstructions that have been derived from two methods. One method is directly comparable to ours in having used an independent reconstruction of BWT which is then subtracted as $\delta^{18}O_T$ from the $\delta^{18}O_b$ record to derive $\delta^{18}O_{sw}$ (Shakun et al., 2015; Sosdian and Rosenthal, 2009; Elderfield et al., 2012; Woodard et al., 2014; Ford and Raymo, 2020; Miller et al., 2020). Other than the Shakun et al. (2015) and Miller et al. (2020) reconstructions, these are based on local records and are thus subject to local temperature and hydrographic effects, and the small number of high-resolution records prevents development of a robust global stack.

The other method takes the opposite approach of ours by first reconstructing sea level and then subtracting it as $\delta^{18}O_{sw}$ from the $\delta^{18}O_b$ record to derive ΔBWT or ΔDOT. Waelbroeck et al. (2002) developed this approach by regressing independently known sea-level data (e.g., from corals) on $\delta^{18}O_b$ for the last glacial cycle and then using this regression (m/‰) to reconstruct sea level from three $\delta^{18}O_b$ records for the last four glacial cycles. They then reconstructed $\delta^{18}O_{sw}$ from sea level using a relation of 0.0085‰ m^{-1}, acknowledging that this relation may not be stationary, and $\delta^{18}O_T$ is then reconstructed by subtracting $\delta^{18}O_{sw}$ from $\delta^{18}O_b$ (see Fig. 3G,H, and I for their ΔBWT reconstructions). Siddall et al. (2010) and Bates et al. (2014) used piece-wise linear relationships between sea-level data and $\delta^{18}O_b$ to reconstruct sea level from ten $\delta^{18}O_b$ records over the last 5 Myr. They then followed the same approach as Waelbroeck et al. (2002) to derive $\delta^{18}O_{sw}$ (using 0.0077‰ m^{-1}) and ΔDOT (see Fig. 3C for their ΔDOT reconstruction). Rohling et al. (2021; 2022) further extended the $\delta^{18}O_b$/sea-level regression using a stack of sea-level records for the last 0.8 Myr (Spratt and Lisiecki, 2016) and the LR04 $\delta^{18}O_b$ stack to reconstruct sea level over the last 40 Myr. Rohling et al. (2021; 2022) also accounted for $\delta^{18}O$ variations in land ice ($\delta^{18}O_i$) over the last glacial cycle which they then applied to their sea-level record to derive $\delta^{18}O_{sw}$ and thus ΔDOT from $\delta^{18}O_b$. We note, however, that applying these regression approaches to a $\delta^{18}O_b$ record to reconstruct sea level reproduces the variability of the $\delta^{18}O_b$ record, which then potentially biases the ΔDOT reconstructions if the relationship between sea level and $\delta^{18}O_b$ is not stationary. Moreover, this approach does not account for the effect of higher temperatures in the Pliocene and early Pleistocene (Fig. 8) on $\delta^{18}O$ of land ice (Winnick and Caves, 2015).

https://doi.org/10.5194/egusphere-2024-3010
Preprint. Discussion started: 27 September 2024

Figure 11 compares our $\delta^{18}O_{sw}$-INT reconstruction with published reconstructions for the last 0.8 Myr, with Figure 11A-E comparing reconstructions derived from existing BWT reconstructions (Ford and Raymo, 2020; Miller et al., 2020; Shakun et al., 2015; Sosdian and Rosenthal, 2009; Elderfield et al., 2012) and Figure 11F comparing one derived from a regression-based sea-level reconstruction (Rohling et al., 2022). In general, there is good agreement between the BWT-derived reconstructions and our reconstruction, although there are some differences with reconstructions based on individual $\delta^{18}O_b$ records during interglaciations, particularly at site 1208 (Fig. 11E) (Ford and Raymo, 2020), which we attribute to some combination of differences in site-specific $\delta^{18}O_T$ and $\delta^{18}O_{sw}$. If the sea-level based $\delta^{18}O_{sw}$ reconstruction (Rohling et al., 2021; Rohling et al., 2022) is a global signal not affected by local temperature or hydrography, then the high agreement between the two reconstructions (Fig. 11F) that were derived by completely independent means provides very high confidence in them. We also note that our LGM (19-26 ka) change in $\delta^{18}O_{sw}$ from modern (0.9±0.1‰) is in agreement with a pore-water based reconstruction (1.0±0.1‰) (Schrag et al., 1996; Schrag et al., 2002).

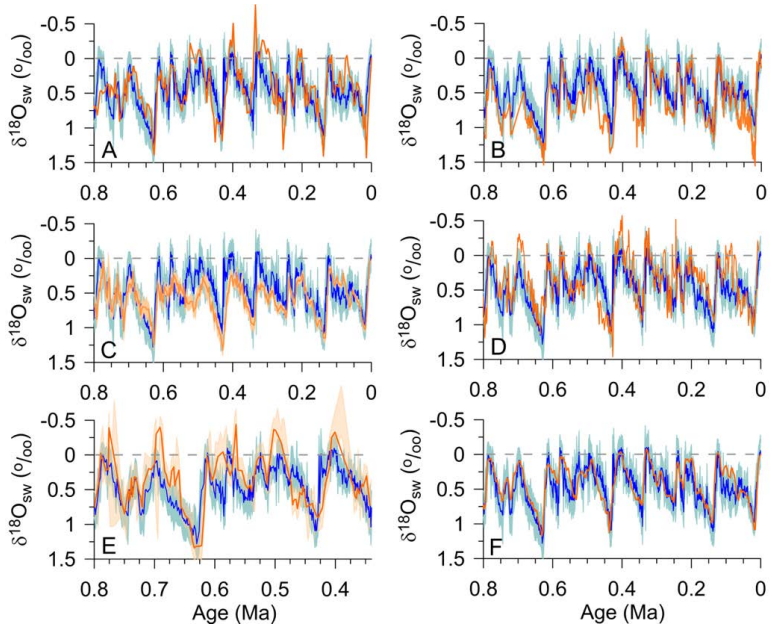

Figure 11. Comparison of our $\delta^{18}O_{sw}$-INT reconstruction (blue) to published $\delta^{18}O_{sw}$ reconstructions (orange). (**A**) Mg/Ca-based $\delta^{18}O_{sw}$ reconstruction from Sosdian and Rosenthal (2009). (**B**) $\delta^{18}O_{sw}$ reconstruction from Miller et al. (2020). (**C**) Proxy-based $\delta^{18}O_{sw}$ reconstruction from Shakun et al. (2015). (**D**) Mg/Ca-based $\delta^{18}O_{sw}$ reconstruction from Elderfield et al. (2012). (**E**) Mg/Ca-based $\delta^{18}O_{sw}$ reconstruction from Ford and Raymo (2020). (**F**) $\delta^{18}O_{sw}$ reconstruction from Rohling et al. (2022). We note that our LGM (19-26 ka) change in $\delta^{18}O_{sw}$ from modern is 0.9±0.1‰, in agreement with a pore-water based reconstruction of 1.0±0.1‰ (Schrag et al., 1996; Schrag et al., 2002).

https://doi.org/10.5194/egusphere-2024-3010
Preprint. Discussion started: 27 September 2024

Figure 12 compares our $\delta^{18}O_{sw}$-INT reconstruction with published reconstructions that span some part or all of the late Pliocene and early Pleistocene. There is a notable difference with the sea-level based reconstruction for times older than 0.9 Ma (Rohling et al., 2021; Rohling et al., 2022) which is primarily expressed by glacial $\delta^{18}O_{sw}$ values being substantially less positive than in our reconstruction, particularly between 3-0.9 Ma (Fig. 12A). We

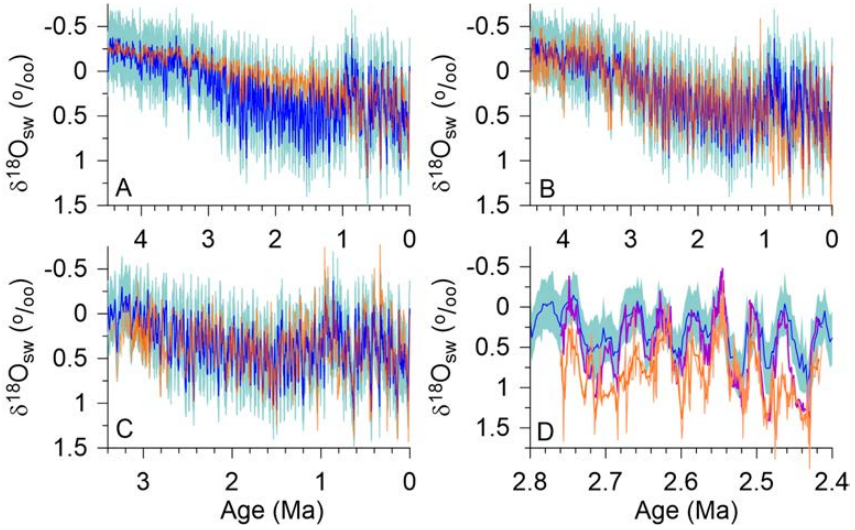

Figure 12. Comparison of our $\delta^{18}O_{sw}$-INT reconstruction (blue) to published $\delta^{18}O_{sw}$ reconstructions (orange). (**A**) $\delta^{18}O_{sw}$ reconstruction from Rohling et al. (2022). (**B**) $\delta^{18}O_{sw}$ reconstruction from Miller et al. (2020). (**C**) Mg/Ca-based $\delta^{18}O_{sw}$ reconstruction from North Atlantic site 607 from Dwyer and Chandler (2009) and Sosdian and Rosenthal (2009). (**D**) Mg/Ca-based $\delta^{18}O_{sw}$ reconstruction from Jakob et al. (2020). The purple line is the published $\delta^{18}O_{sw}$ reconstruction whereas the orange line is the $\delta^{18}O_{sw}$ reconstruction based on recalibrating the Mg/Ca temperature data using Barrientos et al. (2018).

attribute this difference to the previously noted problem with the regression approach used by Rohling et al. (2022; 2021) to reconstruct sea level that preserves the variability of the $\delta^{18}O_b$ record, including the increase in amplitude during the MPT. The Miller et al. (2020) $\delta^{18}O_{sw}$ reconstruction (Fig. 12B) used the smoothed BWT record from Cramer et al. (2011) to extract the $\delta^{18}O_{sw}$ signal, thus assuming that most of the orbital-scale $\delta^{18}O_b$ variability is comprised of $\delta^{18}O_{sw}$. This results in their $\delta^{18}O_{sw}$ reconstruction being in reasonable agreement with our $\delta^{18}O_{sw}$-INT reconstruction, although their early Pleistocene $\delta^{18}O_{sw}$ glacial values tend to be 0.25-0.5‰ more negative than in our reconstruction (Fig. 12B). Figure 12C again compares BWT-based $\delta^{18}O_{sw}$ reconstructions from site 607 (Dwyer and Chandler, 2009; Sosdian and Rosenthal, 2009) that we previously used to gauge the sensitivity of our $\delta^{18}O_{sw}$ reconstruction to changes in HSE and long-term trends in $\delta^{18}O_b$ (Fig. 9). The ostracode-based values for site 607 >3 Ma are on average slightly more positive than our reconstruction (Fig. 12C) which may reflect uncertainties in the Mg/Ca temperature calibration

https://doi.org/10.5194/egusphere-2024-3010
Preprint. Discussion started: 27 September 2024

that requires validation. Otherwise, we emphasize the good agreement between records in their orbital-scale variability. Finally, Figure 12D compares our reconstruction to two reconstructions from North Atlantic site U1313 (Jakob et al., 2020) that differ based on their Mg/Ca calibrations. As with nearby site 607, this record shows good agreement with our reconstruction in the orbital-scale variability, with differences in amplitude reflecting the different Mg/Ca calibrations.

We next compare our ΔMOT and $\delta^{18}O_{sw}$ reconstructions to those from Pacific sites 1123 and 1208 for two intervals when there are substantial differences between their reconstructions and ours (Fig. 13). Of the nine ΔMOT and ΔBWT reconstructions we had previously compared our ΔMOT reconstruction for some or all of the last 0.7 Myr (Fig. 3), these two sites showed the largest differences, with site 1123 having good agreement in its temporal variability but having substantially warmer glacial intervals (Fig. 3D), while site 1208 showed some differences in the timing and amplitude of its variability (Fig. 3F). Figures 13A and 13C also show that temperatures at sites 1123 and 1208 are significantly different than our ΔMOT reconstruction between 0.9-1.4 Ma which spans much of the MPT.

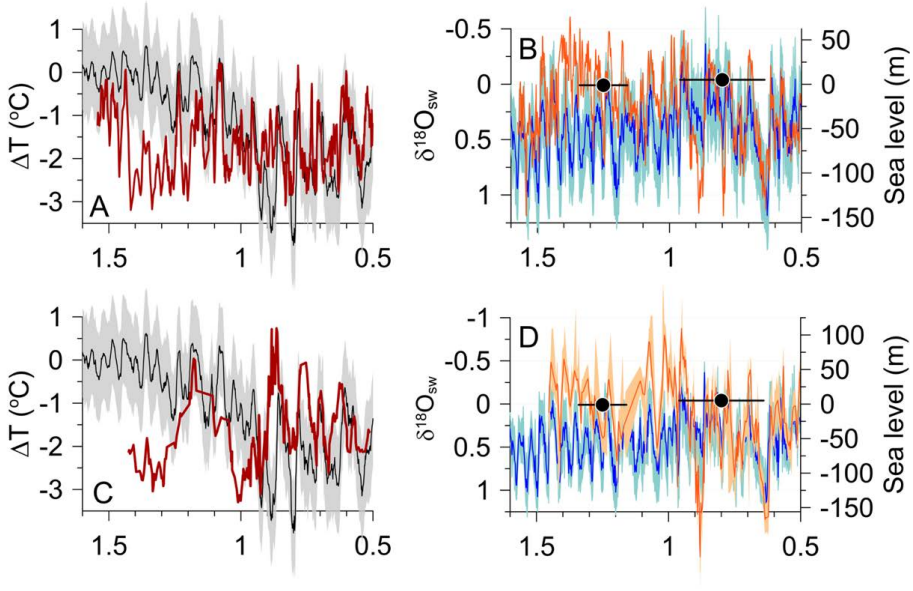

Figure 13. (**A**) Comparison of our ΔMOT reconstruction (black line with 1σ uncertainty) to ΔBWT reconstruction from ODP site 1123 (11-pt running average shown by dark red line) (Elderfield et al., 2012). (**B**) Comparison of our $\delta^{18}O_{sw}$-INT reconstruction (blue line with 1σ uncertainty) to the $\delta^{18}O_{sw}$ reconstruction from ODP site 1123 (orange line) (Elderfield et al., 2012). Black symbols with uncertainies are dated sea-level indicators (Dumitru et al., 2021). (**C**) Comparison of our ΔMOT reconstruction (black line with 1σ uncertainty) to ΔBWT reconstruction from ODP site 1208 (Ford and Raymo, 2020) (5-pt running average shown by dark red line). (**D**) Comparison of our $\delta^{18}O_{sw}$-INT reconstruction (blue line with 1σ uncertainty) to the $\delta^{18}O_{sw}$ reconstruction from ODP site 1208 (orange line with 1σ uncertainty) (Ford and Raymo, 2020). Black symbols with uncertainies are dated sea-level indicators (Dumitru et al., 2021).

https://doi.org/10.5194/egusphere-2024-3010
Preprint. Discussion started: 27 September 2024

These times of temperature differences between the two Pacific sites and our ΔMOT reconstruction result in significant differences in their site-specific $\delta^{18}O_{sw}$ values and our global $\delta^{18}O_{sw}$ reconstruction. Elderfield et al. (2012) and Ford et al. (2020) argued that the more positive $\delta^{18}O_{sw}$ values at sites 1123 and 1208 after 0.9 Ma suggest an increase in ice-sheet volume. Two factors, however, suggest that these changes may instead reflect regional hydrographic changes. The first is that ΔBWTs and $\delta^{18}O_{sw}$ values at the start of the site 1123 record (1.55 Ma) are similar to our reconstructions until ~1.4 Ma when they depart from our reconstructions until ~0.9 Ma, when they then merge again with our reconstructions (Fig. 13A, 13B). This implies that site 1123 is recording large ice sheets before the MPT. The second aspect that suggests that the more-negative $\delta^{18}O_{sw}$ values at these two sites between 1.4-0.9 Ma are not representative of global values is based on their implications for sea-level change. As a first-order approximation, we scale $\delta^{18}O_{sw}$ to sea level using of 0.008‰ m^{-1} as derived from LGM pore water (Schrag et al., 2002) and sea-level (Lambeck et al., 2014) estimates. The scaled pre-MPT $\delta^{18}O_{sw}$ values at the two sites would lead to sea-level highstands that are 50-100 m higher than present throughout much of the 0.9-1.4 Ma interval (Fig. 13B, 13D), thus implying an essentially ice-free world. We thus conclude that the differences in ΔBWT and $\delta^{18}O_{sw}$ at sites 1123 and 1208 from global between 1.4-0.9 Ma reflect regional hydrographic changes (i.e., salinity) that were perhaps associated with the large changes in ocean circulation during the MPT (Lisiecki, 2014; Lang et al., 2016).

4 Processes that contribute to changes in ocean heat storage and mean ocean temperature

During time-dependent climate change, the difference between the radiative forcing at the top of the atmosphere and Earth's radiative response leads to an imbalance in the Earth's energy budget, with a positive imbalance causing the climate system to gain energy and warm and a negative imbalance causing a loss of energy that cools the climate system. Under current anthropogenic climate change, the radiative forcing has exceeded the Earth's radiative response, with 90% of the resulting energy gain being stored in the ocean over the last few decades (Von Schuckmann et al., 2023), thus strongly buffering warming of the atmosphere. The greatest ocean storage over the last century has occurred in the upper 700 m with only weak warming at depths below 2000 m (Von Schuckmann et al., 2023; Cheng et al., 2022) because of the slow transfer of energy into the ocean interior by advection, diffusion, and vertical mixing (Rugenstein et al., 2019; Gregory, 2000; Saenko et al., 2021) so that much of the ocean has not yet reached its equilibrium temperature change and HSE is only ~0.1.

Changes in ocean heat storage similarly play an important role in pacing surface temperature change on longer timescales. On orbital timescales (10^4-10^5 yr), the contribution to the global energy budget from latent heat

https://doi.org/10.5194/egusphere-2024-3010
Preprint. Discussion started: 27 September 2024

fluxes associated with large changes in land ice became comparable to changes in ocean heat storage, with each accounting for ~50% of the increase in the internal energy of the climate system during the last deglaciation (Baggenstos et al., 2019). Changes in some combination of these two energy reservoirs indicate that the global energy budget has rarely been in balance for any extended period throughout the Plio-Pleistocene glacial-interglacial cycles (Shackleton et al., 2023).

Patterns of ocean heat storage since the late 19th century are largely associated with changes in ocean circulation that redistribute heat but do not change global heat content (Bronselaer and Zanna, 2020; Gregory et al., 2016; Cheng et al., 2022). However, observations over the last few decades and climate models show that large-scale patterns of heat storage are increasingly being determined and sustained by heat from anthropogenic surface warming that is added to the ocean interior predominantly along known water mass pathways, with this added heat dominating ocean heat storage change by 2100 (Bronselaer and Zanna, 2020; Fox-Kemper et al., 2021; Cheng et al., 2022). The patterns of ocean heat uptake and storage show most warming occurring in the upper 2000 m between 60ºS and 60ºN, with the majority of heat uptake occurring within wind-driven subduction regions in the Southern Ocean that ventilate the ocean interior (Kuhlbrodt and Gregory, 2012; Gregory et al., 2016), particularly in subantarctic mode water and Antarctic Intermediate Water (Zanna et al., 2019; Cheng et al., 2022), a pattern that persists in equilibrium runs forced by CO_2 quadrupling (Fig. 14A, 14B) (Li et al., 2013). Area-averaged warming in the Pacific Ocean will be smaller than in other basins because of the lack of deepwater formation and limited formation of mode and intermediate water in the North Pacific (Cheng et al., 2022). The increase in Atlantic Ocean heat storage is projected to be nearly equivalent to that of the Pacific but, because of its smaller area, results in a significantly larger area-averaged warming (Cheng et al., 2022).

The temperature of the deep ocean (>2000 m) is largely associated with deepwater formation at high latitudes. Described in broad terms, this process cools the deep ocean at a rate $\nu(T_u-T_d)$, where ν (in s^{-1}) is the volume rate of deepwater formation divided by the volume of the deep ocean, T_d is the temperature of the water sinking at high latitude following convection, and T_u the temperature of water upwelling at lower latitude in the basin[3]. The latter

[3] If the volume V_d of the ocean (in m^3) occupied by deep water is steady, deepwater formation at a rate r_d (in $m^3\ s^{-1}$) must be balanced by an equal rate of removal of deep water by upwelling and mixing with overlying water masses. The rate (in W) at which heat is removed from the deep ocean by this throughput is $r_d(T_u-T_d)\ C$, where C is the volumetric heat capacity of sea water (in $J\ m^{-3}\ ºC^{-1}$). Since the heat capacity of the deep ocean is V_dC ($J\ ºC^{-1}$), its rate of cooling (in $ºC\ s^{-1}$) is $r_d(T_u-T_d)\ C\ /\ (V_dC) = \nu(T_u-T_d)$, where $\nu=r_d/V_d$ whose reciprocal $\tau=1/\nu$ is the time required to renew the entire volume of the deep ocean.

https://doi.org/10.5194/egusphere-2024-3010
Preprint. Discussion started: 27 September 2024

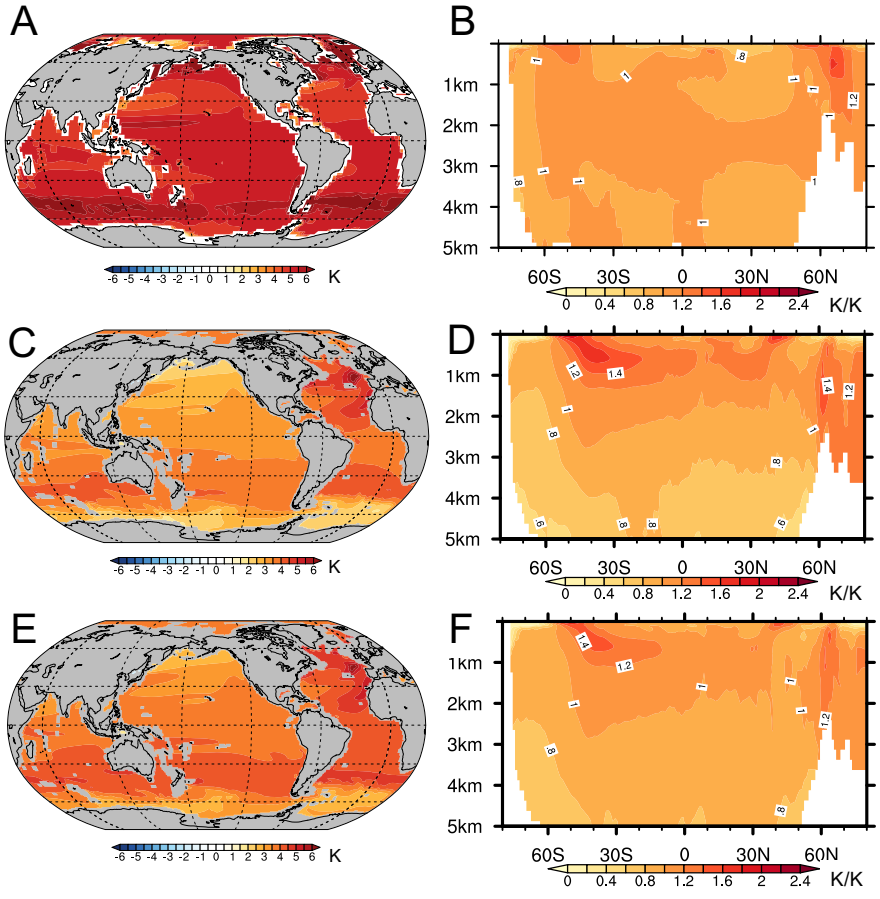

Figure 14. (**A**) Change in 0-2000 m mean equilibrium temperature change (5,900 years) in CESM 1.0.4 for abrupt 4xCO_2 minus preindustrial (Rugenstein et al., 2019). (**B**) Zonal average equilibrium (5,900 years) ocean warming pattern for abrupt 4xCO_2 simulation normalized with the average ocean temperature change (5.12K) (Rugenstein et al., 2019). (**C**) Change in 0-2000 m mean temperature change in iTRACE ICE+ORB+GHG simulation for mid-Holocene (6 ka) minus LGM. (**D**) Zonal average equilibrium ocean warming pattern from iTRACE ICE+ORB+GHG simulation normalized with the average ocean temperature change (3.02K). (**E**) Change in 0-2000 m mean temperature change in iTRACE simulation for mid-Holocene (6 ka) minus LGM. (**F**) Zonal average equilibrium ocean warming pattern from the full iTRACE simulation normalized with the average ocean temperature change (3.6K).

temperature also represents the influence of downward mixing of heat from overlying warmer water at low latitudes. By continuously injecting cold water, the overall effect of the overturning circulation associated with NADW and AABW is to keep the deep ocean cooler than overlying intermediate-depth waters, which are ventilated by lower latitude surface waters. A change in MOT thus occurs from some combination of changes in mid-latitude SSTs (affecting T_u), A change in MOT thus occurs from some combination of changes in mid-latitude SSTs (affecting T_u),

https://doi.org/10.5194/egusphere-2024-3010
Preprint. Discussion started: 27 September 2024

high-latitude SSTs or temperature of the newly formed and sinking deepwater (affecting T_d) and high-latitude deepwater formation rate (ν).

Projected warming in the deep North Atlantic in response to anthropogenic warming is caused by reduction in surface heat loss in that region and in formation of NADW in response to anthropogenic warming (Fox-Kemper et al., 2021). However, NADW does not contribute significantly to global ocean heat uptake (Saenko et al., 2021) and it makes only a small contribution to changes in MOT because it ventilates only a small volume, which is currently ~20% of the global ocean (Johnson, 2008) that decreases during glaciations (Galbraith and De Lavergne, 2019). The correlation between AMOC and ocean heat uptake efficiency across models seems to be due to a common control, such as vertical stratification of the global ocean, rather than to an effect of AMOC on heat uptake (Gregory et al., 2024; Newsom et al., 2023).

In contrast, AABW has a significantly larger influence on MOT than NADW because it ventilates a larger volume, which is currently ~40% of the global ocean (Johnson, 2008) increasing to as much as 80% during glaciations (Galbraith and De Lavergne, 2019). AABW is formed by intense heat loss and brine rejection due to sea-ice formation, with the dense waters sinking, spreading northward to fill much of the abyss, and upwelling as they mix with overlying warm waters especially where in contact with areas of rough seafloor topography. At present, because the temperature of its source waters (T_d in the conceptual model above) remains near the freezing point (~ -1.8ºC), the influence of AABW on abyssal temperatures has been through a reduction in the volume rate of formation (v above) in response to freshening associated with increased meltwater from the Antarctic Ice Sheet (Heuzé et al., 2015; Li et al., 2023) or decreased sea-ice formation (Zhou et al., 2023), allowing more heat to diffuse or mix downwards and warm the deep ocean (Purkey et al., 2019; Johnson et al., 2024). Further global warming and associated sea-ice loss will allow AABW source waters to warm, further contributing to warming of abyssal temperatures (Fig. 14B).

This understanding of the major processes involved in ocean heat uptake and storage in response to GHG emission scenarios over the course of this century (Fox-Kemper et al., 2021; Cheng et al., 2022) or on equilibrium timescales (10^3 yr) (Fig. 14A, 14B) (Rugenstein et al., 2016; Li et al., 2013) contrasts with the longstanding view in paleoceanography that changes in DOT and MOT result solely from SST changes in high-latitude regions where deepwater is formed (Emiliani, 1954; Zachos et al., 2001; Hansen et al., 2023; Evans et al., 2024; Westerhold et al., 2020; Bereiter et al., 2018; Rohling et al., 2022; Hansen et al., 2013). Changes in source water temperature may indeed cause changes in deepwater temperature, for example during substantially warmer climates without Antarctic sea ice

https://doi.org/10.5194/egusphere-2024-3010
Preprint. Discussion started: 27 September 2024

(Goudsmit-Harzevoort et al., 2023; Evans et al., 2024) when AABW could form during Antarctic winter solely by heat loss to the atmosphere without brine rejection, like NADW in the present climate. However, the general notion of a sole control of MOT by SSTs at sites of deepwater formation (affecting T_d) should not be applied regardless of climate state because it neglects the roles of the rate (v) of deepwater formation, as well as the contribution from ocean heat uptake in mid-latitudes, both of which can also affect ocean heat storage (Fig. 14A, 14B) and thus contribute to MOT.

Zhu et al. (2024) used results from the iTRACE simulation of the last deglaciation to assess the role of the primary forcings of Plio-Pleistocene climate change on MOT change. The iTRACE ORB+ICE+GHG simulation includes most of the key forcings during the Plio-Pleistocene ice-age cycles. Orbital forcing has little direct influence on GMSST, leaving ice sheets as the primary forcing that modulates the MOT response to GHG forcing. The effect of retreating Northern Hemisphere ice sheets induces surface warming that is advected downwind to the North Atlantic and North Pacific, further enhancing SST warming (Fig. 15) and ocean heat uptake through ventilation of intermediate waters at 45°N (Fig. 14C, 14D). Since the Southern Ocean is the main region of ocean heat uptake through such wind-driven ventilation, the 0-2000 m average warming is thus significantly enhanced by ice sheets in the ORB+ICE+GHG simulation (Fig. 14C).

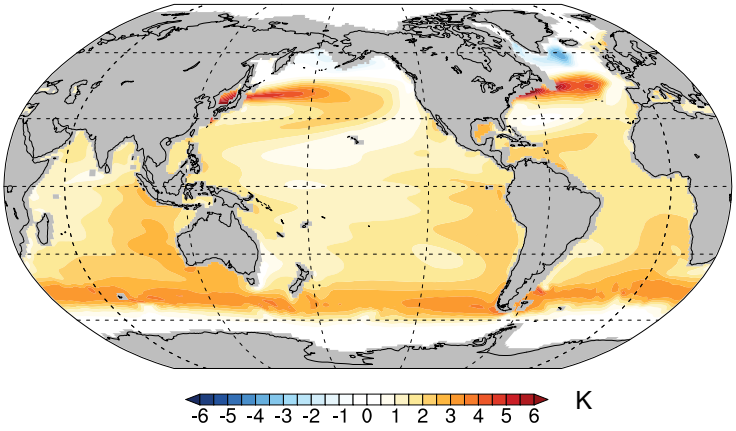

Figure 15. iTRACE ICE-only (ICE run) simulation of ocean surface temperature change (upper 10m) for mid-Holocene (6 ka) minus LGM.

Zhu et al. (2024) found that high-latitude source waters where deepwater is formed are largely covered by sea ice, resulting in their temperature remaining around the freezing point throughout much of the deglaciation. The presence of sea ice results in peak SST warming during deglaciation occurring in mid-to-subpolar latitudes (e.g., Fig.

https://doi.org/10.5194/egusphere-2024-3010
Preprint. Discussion started: 27 September 2024

15) as opposed to peak surface air temperature warming occurring at high latitudes through polar amplification (Zhu et al., 2024). Strong ventilation regions remained co-located with peak SST warming throughout the deglaciation, particularly in the mid-latitudes of the Southern Ocean associated with ventilation of Antarctic Intermediate Water. Figure 14D shows that this was the primary pathway of warming the global ocean, with a negligible warming contribution from reduced AABW formation (Zhu et al., 2024). During the deglaciation, MOT warming lags SST warming by several thousand years, reflecting the timescale of warming the ocean interior by ventilation of intermediate waters and resulting in an average transient HSE ~0.5 that disagrees with proxy records (Zhu et al., 2024). However, the lag is too short to prevent equilibrium MOT warming from being reached during the present interglaciation and HSE reaches ~1.

The full iTRACE simulation includes meltwater forcing (MWF) associated with Heinrich event 1 and the Younger Dryas (He et al., 2021; Gu et al., 2020) and thus captures MOT changes during times of millennial-scale AMOC variability. The strong AMOC weakening in response to MWF causes northward heat transport to decrease, resulting in the characteristic SST bipolar seesaw pattern of Northern Hemisphere cooling and Southern Hemisphere warming. GMSSTs do not change substantially, however, because the effects in both hemispheres on SST nearly cancel each other. In contrast, a suppression of NADW production and reduction of the AMOC generates a subsurface warming that extends to intermediate depths over much of the global ocean (Fig. 14E) and warmed abyssal waters through circulation and mixing processes (Fig. 14F). The MWF causes the subsurface ocean warming that eventually occurs from orbital forcing and land ice on temperature to occur more rapidly. Thus it eliminates the unrealistic lag of MOT behind GMSST, resulting in HSE $\geq$1 throughout the deglaciation, in agreement with proxy records (Zhu et al., 2024).

5 A general hypothesis for the change in ocean heat storage efficiency during the Middle Pleistocene Transition

Based on the understanding of controls on ocean heat uptake and MOT outlined in section 4, we develop a working hypothesis for the reconstructed increase in HSE that occurred during the MPT. The main premise of our simple conceptual model is based on the ocean being comprised of an upper ocean heat reservoir (herein $R_{<2000}$) that extends from roughly 50ºS to 50ºN and to a depth of about 2000 m and has a volume that, in iTRACE, is 43% of the global ocean ($f_{<2000}$ = 0.43), with the heat content and temperature being largely determined by ventilation of mid-latitude surface waters (Fig. 14). The remainder of the ocean (herein $R_{>2000}$), the deeper ocean heat reservoir, is largely below 2000 m that is connected to the surface at latitudes of >50ºS and >50ºN and represents 57% of the global ocean

https://doi.org/10.5194/egusphere-2024-3010
Preprint. Discussion started: 27 September 2024

volume, with the heat content and temperature being largely determined by high-latitude deepwater formation (some combination of T_d and v). In this simple model, ΔMOT is equal to the mean of the changes in temperatures of the upper reservoirs $R_{<2000}$ ($\Delta T_{<2000}$) and deeper reservoir $R_{>2000}$ ($\Delta T_{>2000}$) weighted by their relative ocean volumes ($\Delta MOT = f_{<2000} * \Delta T_{<2000} + (1- f_{<2000}) * \Delta T_{>2000}$).

iTRACE results (Zhu et al., 2024) establish that the average temperature change of the upper reservoir $\Delta T_{<2000}$ is 11%, 16%, and 54% greater than ΔGMSST for scenario ICE+ORB+GHG, the full scenario that includes meltwater forcing, and the ICE-only scenario, respectively. As a simple scaling analysis, we use the full iTRACE scenario to derive upper reservoir $\Delta T_{<2000}$ from the ΔGMSST reconstruction (Fig. 16A) by multiplying it with a factor s=1.16, including $\sigma_{\Delta T<2000} = s * \sigma_{\Delta GMSST}$ (Fig. 16C). The temperature change of the deep reservoir $\Delta T_{>2000}$ is readily derived from the equation for MOT with its uncertainty being the square root of the sum of squares of the individual uncertainties ($\sigma_{>2000} = \sqrt{((\sigma_{\Delta MOT} /(1-f_{<2000}))^2 + (f_{<2000} * s * \sigma_{\Delta GMSST})^2)}$) (Fig. 16D). We assess the sensitivity of upper reservoir $\Delta T_{>2000}$ to different values of $f_{<2000}$ (in the range 0.4-0.6) and of s (1.11-1.54) with all results falling well within the 1σ uncertainty of $\Delta T_{>2000}$. Our sensitivity testing of the iTRACE parameters does not qualitatively change any of our inferences which follow.

Albeit highly idealized, this simple analysis suggests that, for the period from 4.5 Ma until the start of the MPT around 1.5 Ma, $\Delta T_{<2000}$ based on the nominal iTRACE parameters (s=1.16, $f_{<2000}$=0.43) (Fig. 16C) accounts for nearly all of ΔMOT (Fig. 16B) (which in this time window is 50% of ΔGMSST), leaving virtually no change in $\Delta T_{>2000}$ (Fig. 16D) and thus providing an explanation for HSE being ~0.5. In other words, before the MPT, nearly all of ΔMOT is occurring in the upper reservoir, which is ventilated by the wind-driven circulation, and cools along with ΔGMSST. The global cooling trend throughout this period is assumed to be a response to declining CO_2 (Clark et al., 2024) but the cause of it does not affect our argument. Meanwhile, little change is occurring in high-latitude deepwater formation rate (v) and sinking water temperature (T_d) and thus in deep reservoir temperature ($\Delta T_{>2000}$).

The lack of substantial deep reservoir $\Delta T_{>2000}$ change on orbital (10^4-10^5 yr) and geological (10^6 yr) timescales between 4.5-1.5 Ma suggests relatively stable and constant AABW formation, with a subsequent decrease around 1.5 Ma in long-term $\Delta T_{>2000}$ and a rise in its variability suggesting that significant changes in AABW formation had begun. Two lines of evidence support this scenario.

https://doi.org/10.5194/egusphere-2024-3010
Preprint. Discussion started: 27 September 2024

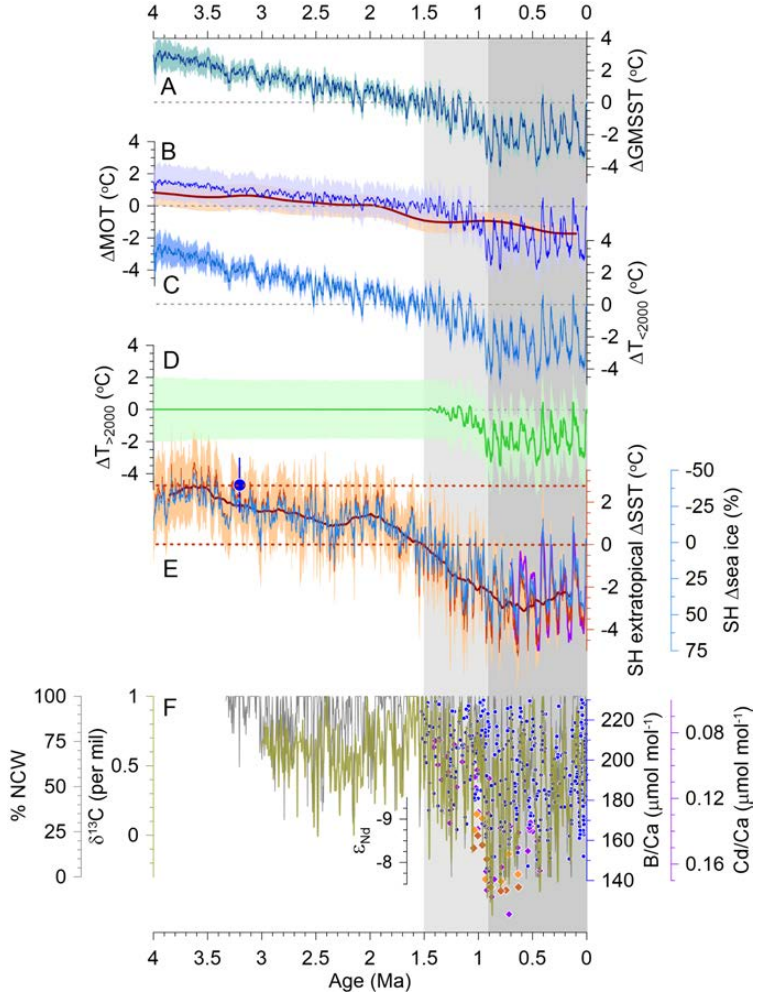

Figure 16. (**A**) Global mean sea surface temperature change from preindustrial (PI) (ΔGMSST) (dark blue line with 1σ uncertainty) (Clark et al., 2024). (**B**) Mean ocean temperature change from PI (ΔMOT) (blue line with 1σ uncertainty) as derived in this paper. Also shown is smoothed ΔBWT reconstruction from Cramer et al. (2011) using their equation 7b (brick-red line with 90% confidence interval). (**C**) ΔT for $R_{<2000}$ area of ocean (43% of global volume) (lighter blue line with 1σ uncertainty) that is on average 16% greater than ΔGMSST ($\Delta T\_R_{<2000}$ = ΔGMSST*1.16) (Zhu et al., 2024). (**D**) ΔT for $R_{>2000}$ area of ocean (57% of global volume) (green line with 1σ uncertainty) derived by $\Delta T\_R_{>2000} = (\Delta MOT - 0.43*\Delta T\_R_{<2000})/0.57$. (**E**) Southern Hemisphere extratropical ΔSST stack (brick-red line with 1σ uncertainty and 201-kyr running average in dark red) (Clark et al., 2024), Southern Ocean Δsea-ice extent derived from relation to Southern Hemisphere extratropical ΔSST stack established by PLIOMIP2 models (Weiffenbach et al., 2024) (light blue line), ΔSST reconstruction for the Southern Ocean for last 0.7 Myr derived from deuterium excess from the Dome Fuji Antarctic ice core (purple = 25-kyr running average) (Uemura et al., 2018), and PLIOMIP2 simulated multi-model mean ΔSST reconstruction for the Southern Ocean during the KM5c time slice at 3.205 Ma shown by blue symbol and 1s uncertainty (2.8±1.3°C) (Weiffenbach et al., 2024). Two red dashed horizontal lines correspond to PLIOMIP2 ΔSST at 3.205 Ma (2.8°C) and at PI (0°C). (**F**) $\delta^{13}C$ stack of mid-to-deep Atlantic cores (green) (Lisiecki, 2014), % Northern Component Water (NCW) (gray) (Lang et al., 2016), ε_{Nd} data from South Atlantic sites ODP 1088 and 1090 (Pena and Goldstein, 2014), and Cd/Ca and B/Ca data from North Atlantic cores CHN82-24-23PC and DSDP 607 (Sosdian et al., 2018; Lear et al., 2016) and South Atlantic site ODP 1267 (Farmer et al., 2019).

https://doi.org/10.5194/egusphere-2024-3010
Preprint. Discussion started: 27 September 2024

First, multi-model results from PLIOMIP2 found that Southern Ocean ΔSSTs for the KM5c interglaciation at 3.205 Ma were 2.8±1.3ºC (Weiffenbach et al., 2024) (Fig. 16E). These warmer SSTs, combined with a simulated increase in precipitation and decrease in sea-ice cover, resulted in a strongly stratified Southern Ocean with relatively uniform warming of 1.5-2.5ºC throughout much of the water column below the low-density surface layer. In 9 of the 15 PLIOMIP2 models, this increase in stratification led to a decrease in AABW formation, with Weiffenbach et al. (2024) noting that four of the other six models also have greater stratification but the AABW response may be modulated by interactions with a stronger AMOC in those models.

To examine whether these mid-Pliocene boundary conditions extended into the Pleistocene, we use the SH extratropical (>30ºS) ΔSST stack from Clark et al. (2024) as a proxy for Southern Ocean SSTs. (Note that this stack only extends to 4 Ma because of the limited number of older records available, and so our analysis here only covers the last 4 Myr.) This inference is supported by the good agreement with the ΔSST reconstruction for the Southern Ocean derived from deuterium excess from the Dome Fuji ice core for the last 0.7 Myr (Uemura et al., 2018) and the PLIOMIP2 multi-model mean Southern Ocean ΔSST of 2.8±1.3ºC at 3.205 Ma (Weiffenbach et al., 2024) compared to the stack's 2.4±1.3ºC (Clark et al., 2024) (Fig. 16E). At the same time, the PLIOMIP2 models find a linear relation between Southern Ocean ΔSST and Δsea-ice area in percentages relative to preindustrial times where Δsea-ice area = -12.4% $^{o}C^{-1}$ *ΔSST (Weiffenbach et al., 2024) which we apply to our ΔSST stack to derive relative changes in sea-ice area over the last 4 Myr (Fig. 16E).

These results suggest that the highly stratified Southern Ocean found in PLIOMIP2 simulations at 3.2 Ma due to warm SSTs and reduced sea-ice extent persisted until ~1.5 Ma. Prior to this, SSTs and sea-ice extent spent 90% of the time above and below, respectively, their preindustrial values. Apparently, SSTs in the AABW formation regions did not decline sufficiently during this interval to affect $\Delta T_{>2000}$ and MOT substantially by lowering T_d. The start of the MPT at 1.5 Ma saw a significant change in the influences on AABW with SSTs spending increasingly more time below preindustrial levels and sea-ice extent spending more time above preindustrial values (~85% during the MPT, ~95% since 0.9 Ma). This might also be related to the proposed decoupling of Southern Ocean vertical mixing and Southern Ocean SST prior to the MPT (KöHler and Bintanja, 2008). We thus conclude that it was the persistence of a highly stratified Southern Ocean that caused a smaller AABW formation rate and persistently warmer T_d than present until ~1.5 Ma, when the gradual decay of stratification and increase in sea-ice extent and variability then enhanced conditions for AABW formation.

https://doi.org/10.5194/egusphere-2024-3010
Preprint. Discussion started: 27 September 2024

Second, deep-ocean water masses show changes that are consistent with changes in AABW formation inferred from our simple model, i.e. v increased at that time. Starting at ~1.5 Ma, there was an increasing frequency of southern component waters (e.g. AABW) (Lang et al., 2016) which are depleted in $\delta^{13}C$ (Lisiecki, 2014), recording a growing influence of AABW at the expense of NADW in the Atlantic Ocean (Fig. 16F). This was followed by a further step-change increase in the relative share of $\delta^{13}C$-depleted AABW during glacial climates around 0.9 Ma, as also indicated by a rapid increase in ε_{Nd} values (Pena and Goldstein, 2014) and an increase in nutrient content and a decrease in carbonate-ion saturation (Lear et al., 2016; Sosdian et al., 2018; Farmer et al., 2019) (Fig. 16F).

After the MPT, ΔMOT variability was greater than before, exceeding the contribution from upper reservoir $\Delta T_{<2000}$. During the glacial cycles of the last 0.8 Myr, proxy records suggest that v has varied along with ΔGMSST (Fig. 16F) (Clark et al., 2024). Without requiring any long-term change in T_d, which has remained near freezing, this can explain synchronized variations in $\Delta T_{<2000}$ and $\Delta T_{>2000}$, leading finally to an HSE of ~1 during this period.

6 Summary

When compared to a reconstruction of ΔGMSST over the last 4.5 Myr, high-fidelity proxies of deep (>200 m) ocean temperature change show good agreement in orbital-scale amplitude and long-term trend over the last 0.7 Ma but their long-term trends are ~50% of long-term ΔGMSST beyond 1.5 Ma, suggesting an increase of HSE from ~0.5 to ~1 during the MPT (1.5-0.9 Ma). This increase is further supported when assuming that HSE was 1 throughout the last 4.5 Myr and applying this temperature history (as $\delta^{18}O_T$) to isolate the seawater component ($\delta^{18}O_{sw}$) of a probabilistic global $\delta^{18}O_b$ stack (Prob-stack). Under this scenario, Pliocene $\delta^{18}O_{sw}$ values are 0.3‰ to 0.5‰ despite robust evidence for higher-than-present Pliocene sea level that require values in $\delta^{18}O_{sw}$ to be smaller than 0‰, suggesting that too much of the $\delta^{18}O_b$ signal is being removed by the $\delta^{18}O_T$ component using an HSE of 1. Applying our ΔMOT reconstruction where HSE increases from 0.5 to 1 across the MPT results in early Pleistocene and Pliocene $\delta^{18}O_{sw}$ values (0‰ to -0.1‰) that continue to be more positive than multiple data constraints. While a further decrease in HSE to 0.1 would result in average Pliocene $\delta^{18}O_{sw}$ values of -0.2‰ which could explain higher sea levels at that time, such a low HSE is ruled out by proxy-based bottom water temperature reconstructions. We therefore adopt the hypothesis that there has been a diagenetic overprint on $\delta^{18}O_b$ records that average to a long-term secular increase of between 0.05‰ Myr^{-1} to 0.12‰ Myr^{-1} which, when removed from the Prob-stack, results in Pliocene $\delta^{18}O_{sw}$ values of -0.1‰ to -0.4‰ that are consistent with sea-level highstands of 20-25 m above present.

https://doi.org/10.5194/egusphere-2024-3010
Preprint. Discussion started: 27 September 2024

To explain the increase in HSE across the MPT, we develop a simple conceptual model that considers the ocean as being comprised of an upper non-polar ocean reservoir with the temperature being largely determined by ventilation of mid-latitude surface waters and a deeper ocean reservoir whose temperature is largely determined by high-latitude deepwater formation. Using results from a transient simulation of the last deglaciation with a global climate model, we develop a simple scaling analysis to derive upper reservoir ΔT from the ΔGMSST reconstruction which is then subtracted from ΔMOT to derive deep reservoir ΔT. This analysis suggests that before the MPT, nearly all of ΔMOT is occurring in the upper reservoir through changes in wind-driven ventilation and little is occurring in the deep reservoir from changes in deepwater formation, resulting in HSE being ~0.5. Around 1.5 Ma, the amplitude of ΔMOT variability begins to increase and exceeds the contribution from upper reservoir ΔT, thus requiring an increasing contribution of lower reservoir ΔT to ΔMOT through an increase in deepwater formation that leads to an HSE of ~1 over the last 0.8 Myr. We attribute these changes in deepwater formation to long-term cooling which caused a transition starting ~1.5 Ma from a highly stratified Southern Ocean due to warm SSTs and reduced sea-ice extent to colder SSTs with a significant increase in sea-ice extent and more vertical exchange of water masses.

.

Data Availability Statement: Data archiving is underway at the NOAA Paleoclimatology web site: https://www.ncei.noaa.gov/products/paleoclimatology.

Author contribution: Conceptualization: PUC, JDS. Methodology: PUC, JDS, YR, CZ, DPS, PK. Investigation: PUC, JDS, YR, CZ, JMG, PK, ZL, DPS, PJB. Writing – original draft: PUC, JDS, YR. Writing – review & editing: PUC, JDS, YR, JMG, PK, CZ, ZL, PJB, DPS.

Competing interests. The authors declare that they have no conflict of interest.

Acknowledgments: We thank the paleoclimate and paleoceanographic communities for making their data sets widely available, the National Centers for Environmental Information of NOAA and the World Data Center PANGAEA for archiving data, and Chris Brierley, Julia Tindall, and Julia E. Weiffenbach for providing climate model data. This publication contributed to Beyond EPICA, a project of the European Union's Horizon 2020 research and innovation program (Oldest Ice Core). P.U.C is funded by National Science Foundation OPP-2103032, Y.R. is supported by National Science Foundation OCE-1834208, and Z.L. is supported by National Science Foundation OCE-1810681.

https://doi.org/10.5194/egusphere-2024-3010
Preprint. Discussion started: 27 September 2024

References

Ahn, S., Khider, D., Lisiecki, L. E., and Lawrence, C. E.: A probabilistic Pliocene–Pleistocene stack of benthic $\delta^{18}O$ using a profile hidden Markov model, Dynamics and Statistics of the Climate System, 2, 1-16, 2017.

Alder, J. R. and Hostetler, S. W.: Global climate simulations at 3000-year intervals for the last 21 000 years with the GENMOM coupled atmosphere-ocean model, Climate of the Past, 11, 449-471, 10.5194/cp-11-449-2015, 2015.

Baggenstos, D., Haberli, M., Schmitt, J., Shackleton, S. A., Birner, B., Severinghaus, J. P., Kellerhals, T., and Fischer, H.: Earth's radiative imbalance from the Last Glacial Maximum to the present, Proceedings of the National Academy of Sciences of the United States of America, 116, 14881-14886, 10.1073/pnas.1905447116, 2019.

Barrientos, N., Lear, C. H., Jakobsson, M., Stranne, C., O'Regan, M., Cronin, T. M., Gukov, A. Y., and Coxall, H. K.: Arctic Ocean benthic foraminifera Mg/Ca ratios and global Mg/Ca-temperature calibrations: New constraints at low temperatures, Geochimica et Cosmochimica Acta, 236, 240-259, 10.1016/j.gca.2018.02.036, 2018.

Bates, S. L., Siddall, M., and Waelbroeck, C.: Hydrographic variations in deep ocean temperature over the mid-Pleistocene transition, Quaternary Science Reviews, 88, 147-158, 10.1016/j.quascirev.2014.01.020, 2014.

Bereiter, B., Shackleton, S., Baggenstos, D., Kawamura, K., and Severinghaus, J.: Mean global ocean temperatures during the last glacial transition, Nature, 553, 39-44, 10.1038/nature25152, 2018.

Bijma, J., Spero, H. J., and Lea, D. W.: Reassessing foraminiferal stable isotope geochemistry: Impact of the oceanic carbonate system (experimental results), in: Use of Proxies in Paleoceanography: Examples from the South Atlantic, edited by: Fischer, G., and Wefer, G., Springer-Verlag, Berlin, 489-512, 1999.

Braconnot, P., Harrison, S. P., Kageyama, M., Bartlein, P. J., Masson-Delmotte, V., Abe-Ouchi, A., Otto-Bliesner, B., and Zhao, Y.: Evaluation of climate models using palaeoclimatic data, Nature Climate Change, 2, 417-424, 10.1038/nclimate1456, 2012.

Bronselaer, B. and Zanna, L.: Heat and carbon coupling reveals ocean warming due to circulation changes, Nature, 584, 227-+, 10.1038/s41586-020-2573-5, 2020.

Cheng, L. J., von Schuckmann, K., Abraham, J. P., Trenberth, K. E., Mann, M. E., Zanna, L., England, M. H., Zika, J. D., Fasullo, J. T., Yu, Y. Q., Pan, Y. Y., Zhu, J., News, E. R., Bronselaer, B., and Lin, X. P.: Past and future ocean warming, Nature Reviews Earth & Environment, 3, 776-794, 10.1038/s43017-022-00345-1, 2022.

Church, J. A., Clark, P. U., Cazenave, A., Gregory, J. M., Jevrejeva, S., Levermann, A., Merrifield, M. A., Milne, G. A., Nerem, R. S., Nunn, P. D., Payne, A. J., Pfeffer, W. T., Stammer, D., and Unnikrishnan, A. S.: Sea Level Change, in: Climate Change 2013: The Physical Science Basis. Contribution of Working Group I to the Fifth Assessment Report of the Intergovernmental Panel on Climate Change, edited by: Stocker, T. F., Qin, D., Plattner, G.-K., Tignor, M., Allen, S. K., Boschung, J., Nauels, A., Xia, Y., Bex, V., and Midgley, P. M., Cambridge University Press, Cambridge, United Kingdom and New York, NY, USA, 1137-1216, 2013.

Clark, P. U., Shakun, J. D., Rosenthal, Y., Köhler, P., and Bartlein, P. J.: Global and regional temperature change over the last 4.5 million years, Science, 383, 884-890, 2024.

Clark, P. U., Shakun, J. D., Marcott, S. A., Mix, A. C., Eby, M., Kulp, S., Levermann, A., Milne, G. A., Pfister, P. L., Santer, B. D., Schrag, D. P., Solomon, S., Stocker, T. F., Strauss, B. H., Weaver, A. J., Winkelmann, R., Archer, D., Bard, E., Goldner, A., Lambeck, K., Pierrehumbert, R. T., and Plattner, G. K.: Consequences of twenty-first-century policy for multi-millennial climate and sea-level change, Nature Climate Change, 6, 360-369, 10.1038/nclimate2923, 2016.

Cramer, B. S., Miller, K. G., Barrett, P. J., and Wright, J. D.: Late Cretaceous-Neogene trends in deep ocean temperature and continental ice volume: Reconciling records of benthic foraminiferal geochemistry (delta O-18 and Mg/Ca) with sea level history, Journal of Geophysical Research-Oceans, 116, 10.1029/2011jc007255, 2011.

de Boer, B., Lourens, L. J., and van de Wal, R. S. W.: Persistent 400,000-year variability of Antarctic ice volume and the carbon cycle is revealed throughout the Plio-Pleistocene, Nature Communications, 5, 10.1038/ncomms3999, 2014.

Dumitru, O. A., Austermann, J., Polyak, V. J., Fornos, J. J., Asmerom, Y., Gines, J., Gines, A., and Onac, B. P.: Constraints on global mean sea level during Pliocene warmth, Nature, 574, 233-236, 10.1038/s41586-019-1543-2, 2019.

Dumitru, O. A., Austermann, J., Polyak, V. J., Fornos, J. J., Asmerom, Y., Gines, J., Gines, A., and Onac, B. P.: Sea-level stands from the Western Mediterranean over the past 6.5 million years, Sci Rep-Uk, 11, 6681, 10.1038/s41598-020-80025-6, 2021.

Dwyer, G. S. and Chandler, M. A.: Mid-Pliocene sea level and continental ice volume based on coupled benthic Mg/Ca palaeotemperatures and oxygen isotopes, Philosophical Transactions of the Royal Society A-Mathematical Physical and Engineering Sciences, 367, 157-168, 10.1098/rsta.2008.0222, 2009.

https://doi.org/10.5194/egusphere-2024-3010
Preprint. Discussion started: 27 September 2024

Elderfield, H., Ferretti, P., Greaves, M., Crowhurst, S., McCave, I. N., Hodell, D., and Piotrowski, A. M.: Evolution of ocean temperature and ice volume through the mid-Pleistocene climate transition, Science, 337, 704-709, 10.1126/science.1221294, 2012.

Elderfield, H., Greaves, M., Barker, S., Hall, I. R., Tripati, A., Ferretti, P., Crowhurst, S., Booth, L., and Daunt, C.: A record of bottom water temperature and seawater delta(18)O for the Southern Ocean over the past 440 kyr based on Mg/Ca of benthic foraminiferal Uvigerina spp, Quaternary Science Reviews, 29, 160-169, 10.1016/j.quascirev.2009.07.013, 2010.

Emiliani, C.: Temperatures of Pacific bottom waters and polar superficial waters during the Tertiary, Science, 119, 853-855, 1954.

Evans, D. and Müller, W.: Deep time foraminifera Mg/Ca paleothermometry: Nonlinear correction for secular change in seawater Mg/Ca, Paleoceanography, 27, PA4205, 10.1029/2012pa002315, 2012.

Evans, D., Brugger, J., Inglis, G. N., and Valdes, P.: The temperature of the deep ocean Is a robust proxy for global mean surface temperature during the Cenozoic, Paleoceanography and Paleoclimatology, 39, e2023PA004788, 2024.

Farmer, J. R., Honisch, B., Haynes, L. L., Kroon, D., Jung, S., Ford, H. L., Raymo, M. E., Jaume-Segui, M., Bell, D. B., Goldstein, S. L., Pena, L. D., Yehudai, M., and Kim, J.: Deep Atlantic Ocean carbon storage and the rise of 100,000-year glacial cycles, Nature Geoscience, 12, 355-360, 10.1038/s41561-019-0334-6, 2019.

Ford, H. L. and Raymo, M. E.: Regional and global signals in seawater $\delta^{18}O$ records across the mid-Pleistocene transition, Geology, 48, 113-117, 10.1130/g46546.1, 2020.

Ford, H. L., Sosdian, S. M., Rosenthal, Y., and Raymo, M. E.: Gradual and abrupt changes during the Mid-Pleistocene Transition, Quaternary Science Reviews, 148, 222-233, https://doi.org/10.1016/j.quascirev.2016.07.005, 2016.

Fox-Kemper, B., Hewitt, H., Xiao, C., Aðalgeirsdóttir, G., Drijfhout, S. S., Edwards, T. L., Golledge, N. R., Hemer, M., Kopp, R. E., Krinner, G., Mix, A., Notz, D., Nowicki, S., Nurhati, I. S., Ruiz, L., Sallée, J.-B., Slangen, A. B. A., and Yu, Y.: Ocean, Cryosphere, and Sea Level Change, in: Climate Change 2021: The Physical Science Basis. Contribution of Working Group I to the Sixth Assessment Report of the Intergovernmental Panel on Climate Change, edited by: Masson-Delmotte, V., Zhai, P., Pirani, A., Connors, S. L., Péan, C., Berger, S., Caud, N., Chen, L., Goldfarb, L., Gomis, M. I., Huang, M., Leitzell, K., Lonnoy, E., Matthews, J. B. R., Maycock, T., Waterfield, T., Yelekçi, O., Yu, R., and Zhou, B., Cambriidge University Press, Cambridge, UK, 1211-1362, 2021.

Friedrich, T. and Timmermann, A.: Using Late Pleistocene sea surface temperature reconstructions to constrain future greenhouse warming, Earth and Planetary Science Letters, 530, 10.1016/j.epsl.2019.115911, 2020.

Galbraith, E. and de Lavergne, C.: Response of a comprehensive climate model to a broad range of external forcings: relevance for deep ocean ventilation and the development of late Cenozoic ice ages, Climate Dynamics, 52, 653-679, 10.1007/s00382-018-4157-8, 2019.

Gasson, E., DeConto, R. M., and Pollard, D.: Modeling the oxygen isotope composition of the Antarctic ice sheet and its significance to Pliocene sea level, Geology, 44, 827-830, 10.1130/g38104.1, 2016.

Goudsmit-Harzevoort, B., Lansu, A., Baatsen, M. L. J., von der Heydt, A. S., de Winter, N. J., Zhang, Y. R., Abe-Ouchi, A., de Boer, A., Chan, W. L., Donnadieu, Y., Hutchinson, D. K., Knorr, G., Ladant, J. B., Morozova, P., Niezgodzki, I., Steinig, S., Tripati, A., Zhang, Z. S., Zhu, J., and Ziegler, M.: The Relationship Between the Global Mean Deep-Sea and Surface Temperature During the Early Eocene, Paleoceanography and Paleoclimatology, 38, 10.1029/2022pa004532, 2023.

Gray, W. R., de Lavergne, C., Wills, R. J. C., Menviel, L., Spence, P., Holzer, M., Kageyama, M., and Michel, E.: Poleward Shift in the Southern Hemisphere Westerly Winds Synchronous With the Deglacial Rise in CO₂, Paleoceanography and Paleoclimatology, 38, 10.1029/2023pa004666, 2023.

Gregory, J. M.: Vertical heat transports in the ocean and their effect on time-dependent climate change, Climate Dynamics, 16, 501-515, 2000.

Gregory, J. M., Stouffer, R. J., Raper, S. C. B., Stott, P. A., and Rayner, N. A.: An observationally based estimate of the climate sensitivity, Journal of Climate, 15, 3117-3121, 10.1175/1520-0442(2002)015<3117:Aobeot>2.0.Co;2, 2002.

Gregory, J. M., Bloch-Johnson, J., Couldrey, M. P., Exarchou, E., Griffies, S. M., Kuhlbrodt, T., Newsom, E., Saenko, O. A., Suzuki, T., Wu, Q. R., Urakawa, S., and Zanna, L.: A new conceptual model of global ocean heat uptake, Climate Dynamics, 62, 1669-1713, 10.1007/s00382-023-06989-z, 2024.

Gregory, J. M., Bouttes, N., Griffies, S. M., Haak, H., Hurlin, W. J., Jungclaus, J., Kelley, M., Lee, W. G., Marshall, J., Romanou, A., Saenko, O. A., Stammer, D., and Winton, M.: The Flux-Anomaly-Forced Model Intercomparison Project (FAFMIP) contribution to CMIP6: investigation of sea-level and ocean climate change in response to CO2 forcing, Geosci. Model Dev., 9, 3993-4017, 10.5194/gmd-9-3993-2016, 2016.

https://doi.org/10.5194/egusphere-2024-3010
Preprint. Discussion started: 27 September 2024

Gu, S., Liu, Z., Oppo, D. W., Lynch-Stieglitz, J., Jahn, A., Zhang, J., and Wu, L.: Assessing the potential capability of reconstructing glacial Atlantic water masses and AMOC using multiple proxies in CESM, Earth and Planetary Science Letters, 541, 116294, 10.1016/j.epsl.2020.116294, 2020.

Haeberli, M., Baggenstos, D., Schmitt, J., Grimmer, M., Michel, A., Kellerhals, T., and Fischer, H.: Snapshots of mean ocean temperature over the last 700 000 years using noble gases in the EPICA Dome C ice core, Climate of the Past, 17, 843-867, 2021.

Hansen, J., Sato, M., Russell, G., and Kharecha, P.: Climate sensitivity, sea level and atmospheric carbon dioxide, Philosophical Transactions of the Royal Society A-Mathematical Physical and Engineering Sciences, 371, 10.1098/rsta.2012.0294, 10.1098/rsta.2012.0294, 2013.

Hansen, J. E., Sato, M., Simons, L., Nazarenko, L. S., Sangha, I., Kharecha, P., Zachos, J. C., von Schuckmann, K., Loeb, N. G., Osman, M. B., Jin, Q., Tselioudis, G., Jeong, E., Lacis, A., Ruedy, R., Russell, G., Cao, J., and Li, J.: Global warming in the pipeline, Oxford Open Climate Change, 3, kgad008, 2023.

He, C., Liu, Z., Otto-Bliesner, B. L., Brady, E. C., Zhu, C., Tomas, R., Clark, P. U., Zhu, J., Jahn, A., Gu, S., Zhang, J., Nusbaumer, J., Noone, D., Cheng, H., Wang, Y., Yan, M., and Bao, Y.: Hydroclimate footprint of pan-Asian monsoon water isotope during the last deglaciation, Science Advances, 7, eabe2611, 10.1126/sciadv.abe2611, 2021.

Heuzé, C., Heywood, K. J., Stevens, D. P., and Ridley, J. K.: Changes in global ocean bottom properties and volume transports in CMIP5 models under climate change scenarios, Journal of Climate, 28, 2917-2944, 2015.

Jakob, K. A., Wilson, P. A., Pross, J., Ezard, T. H. G., Fiebig, J., Repschlager, J., and Friedrich, O.: A new sea-level record for the Neogene/Quaternary boundary reveals transition to a more stable East Antarctic Ice Sheet, Proceedings of the National Academy of Sciences of the United States of America, 117, 30980-30987, 10.1073/pnas.2004209117, 2020.

Johnson, G. C.: Quantifying Antarctic Bottom Water and North Atlantic Deep Water volumes, Journal of Geophysical Research, 113, C05027, 2008.

Johnson, G. C., Sadman Mahmud, A. K. M., Macdonald, A. M., and Twining, B. S.: Antarctic Bottom Water warming, freshening, and contraction in the eastern Bellingshausen Basin, Geophysical Research Letters, 51, e2024GL109937, 2024.

Kim, S. T. and O'Neil, J. R.: Equilibrium and nonequilibrium oxygen isotope effects in synthetic carbonates, Geochimica et Cosmochimica Acta, 61, 3461-3475, 10.1016/s0016-7037(97)00169-5, 1997.

Köhler, P.: Atmospheric CO_2 concentration based on boron isotopes versus simulations of the global carbon cycle during the Plio-Pleistocene, Paleoceanography and Paleoclimatology, 38, e2022PA004439, 2023.

Köhler, P. and Mulitza, S.: No detectable influence of the carbonate ion effect on changes in stable carbon isotope ratios (δ13C) of shallow dwelling planktic foraminifera over the past 160 kyr, Clim. Past, 20, 991-1015, 10.5194/cp-20-991-2024, 2024.

Köhler, P. and Bintanja, R.: The carbon cycle during the Mid Pleistocene Transition: the Southern Ocean decoupling hypothesis, Climate of the Past, 4, 311-332, 10.5194/cp-4-311-2008, 2008.

Kuhlbrodt, T. and Gregory, J. M.: Ocean heat uptake and its consequences for the magnitude of sea level rise and climate change, Geophysical Research Letters, 39, 10.1029/2012gl052952, 2012.

Lambeck, K., Rouby, H., Purcell, A., Sun, Y., and Sambridge, M.: Sea level and global ice volumes from the Last Glacial Maximum to the Holocene, Proceedings of the National Academy of Sciences, 111, 15296-15303, 2014.

Lang, D. C., Bailey, I., Wilson, P. A., Chalk, T. B., Foster, G. L., and Gutjahr, M.: Incursions of southern-sourced water into the deep North Atlantic during late Pliocene glacial intensification, Nature Geoscience, 9, 375-379, 10.1038/ngeo2688, 2016.

Lear, C. H., Rosenthal, Y., and Wright, J. D.: The closing of a seaway: ocean water masses and global climate change, Earth and Planetary Science Letters, 210, 425-436, 10.1016/s0012-821x(03)00164-x, 2003.

Lear, C. H., Billups, K., Rickaby, R. E. M., Diester-Haass, L., Mawbey, E. M., and Sosdian, S. M.: Breathing more deeply: Deep ocean carbon storage during the mid-Pleistocene climate transition, Geology, 44, 1035-1038, 10.1130/g38636.1, 2016.

Li, C., von Storch, J.-S., and Marotzke, J.: Deep-ocean heat uptake and equilibrium climate response, Climate Dynamics, 40, 1071–1086, 2013.

Li, Q., England, M. H., Hogg, A. M., Rintoul, S. R., and Morrison, A. K.: Abyssal ocean overturning slowdown and warming driven by Antarctic meltwater, Nature, 615, 841-847, 2023.

Lisiecki, L. E.: Atlantic overturning responses to obliquity and precession over the last 3 Myr, Paleoceanography, 29, 71-86, 10.1002/2013pa002505, 2014.

Lisiecki, L. E. and Raymo, M. E.: A Pliocene-Pleistocene stack of 57 globally distributed benthic $\delta^{18}O$ records, Paleoceanography, 20, 2004PA001071, 2005.

https://doi.org/10.5194/egusphere-2024-3010
Preprint. Discussion started: 27 September 2024

Marchitto, T. M., Curry, W. B., Lynch-Stieglitz, J., Bryan, S. P., Cobb, K. M., and Lund, D. C.: Improved oxygen isotope temperature calibrations for cosmopolitan benthic foraminifera, Geochimica Cosmochimica Acta, 130, 1-11, 2014.

Martin, P. A., Lea, D. W., Rosenthal, Y., Papenfuss, T. P., and Sarnthein, M.: Late Quaternary Deep-Sea Temperatures Inferred From Benthic Foraminiferal Magnesium, Earth Planetary Science Letters, 198, 193-209, 2002.

Meinicke, N., Reimi, M. A., Ravelo, A. C., and Meckler, A. N.: Coupled Mg/Ca and clumped isotope measurements indicate lack of substantial mixed layer cooling in the western Pacific warm pool during the last 5 Million years, Paleoceanography and Paleoclimatology, 36, e2020PA004115, 10.1029/2020pa004115, 2021.

Miller, K. G., Browning, J. V., Schmelz, W. J., Kopp, R. E., Mountain, G. S., and Wright, J. D.: Cenozoic sea-level and cryospheric evolution from deep-sea geochemical and continental margin records, Science Advances, 6, 10.1126/sciadv.aaz1346, 2020.

Miller, K. G., Wright, J. D., Browning, J. V., Kulpecz, A., Kominz, M., Naish, T. R., Cramer, B. S., Rosenthal, Y., Peltier, W. R., and Sosdian, S.: High tide of the warm Pliocene: Implications of global sea level for Antarctic deglaciation, Geology, 40, 407-410, 10.1130/g32869.1, 2012.

Nederbragt, A. J.: The effect of seawater carbonate chemistry on the stable isotope composition of Cibicidoides wuellerstorfi and other Cibicidoides species, Paleoceanography and Paleoclimatology, 38, e2023PA004667, 2023.

Newsom, E., Zanna, L., and Gregory, J.: Background pycnocline depth constrains future ocean heat uptake ffficiency, Geophysical Research Letters, 50, 10.1029/2023gl105673, 2023.

Pena, L. D. and Goldstein, S. L.: Thermohaline circulation crisis and impacts during the mid-Pleistocene transition, Science, 345, 318-322, 10.1126/science.1249770, 2014.

Pöppelmeier, F., Baggenstos, D., Grimmer, M., Liu, Z. J., Schmitt, J., Fischer, H., and Stocker, T. F.: The Effect of Past Saturation Changes on Noble Gas Reconstructions of Mean Ocean Temperature, Geophysical Research Letters, 50, 10.1029/2022gl102055, 2023.

Purkey, S. G., Johnson, G. C., Talley, L. D., Sloyan, B. M., Wijffels, S. E., Smethie, W., Mecking, S., and Katsumata, K.: Unabated bottom water warming and freshening in the South Pacific Ocean, Journal of Geophysical Research-Oceans, 124, 1778-1794, 2019.

Rathmann, S., Hess, S., Kuhnert, H., and Mulitza, S.: Mg/Ca ratios of the benthic foraminifera Oridorsalis umbonatus obtained by laser ablation from core top sediments:: Relationship to bottom water temperature -: art. no. Q12013, Geochemistry Geophysics Geosystems, 5, 10.1029/2004gc000808, 2004.

Raymo, M. E., Kozdon, R., Evans, D., Lisiecki, L., and Ford, H. L.: The accuracy of mid-Pliocene δ^{18}O-based ice volume and sea level reconstructions, Earth-Science Reviews, 177, 291-302, 10.1016/j.earscirev.2017.11.022, 2018.

Rohling, E. J., Yu, J. M., Heslop, D., Foster, G. L., Opdyke, B., and Roberts, A. P.: Sea level and deep-sea temperature reconstructions suggest quasi-stable states and critical transitions over the past 40 million years, Science Advances, 7, eabf5326, 10.1126/sciadv.abf5326, 2021.

Rohling, E. J., Foster, G. L., Gernon, T. M., Grant, K. M., Heslop, D., Hibbert, F. D., Roberts, A. P., and Yu, J.: Comparison and synthesis of sea-level and deep-sea temperature variations over the past 40 million years, Reviews of Geophysics, 60, e2022RG000775, doi.org/10.1029/2022RG000775, 2022.

Rosenthal, Y., Bova, S., and Zhou, X. L.: A user guide for choosing planktic foraminiferal Mg/Ca-temperature calibrations, Paleoceanography and Paleoclimatology, 37, e2022PA004413, 10.1029/2022pa004413, 2022.

Rugenstein, M., Bloch-Johnson, J., Abe-Ouchi, A., Andrews, T., Beyerle, U., Cao, L., Chadha, T., Danabasoglu, G., Dufresne, J. L., Duan, L., Foujols, M. A., Frolicher, T., Geoffroy, O., Gregory, J., Knutti, R., Li, C., Marzocchi, A., Mauritsen, T., Menary, M., Moyer, E., Nazarenko, L., Paynter, D., Saint-Martin, D., Schmidt, G. A., Yamamoto, A., and Yang, S. T.: LongRunMIP: Motivation and Design for a Large Collection of Millennial-Length AOGCM Simulations, Bulletin of the American Meteorological Society, 100, 2551-2570, 10.1175/bams-d-19-0068.1, 2019.

Rugenstein, M. A. A., Sedlácek, J., and Knutti, R.: Nonlinearities in patterns of long-term ocean warming, Geophysical Research Letters, 43, 3380-3388, 10.1002/2016gl068041, 2016.

Saenko, O., Gregory, J. M., Griffies, S. M., Couldrey, M. P., and Dias, F. B.: Contribution of ocean physics and dynamics at different scales to heat uptaken in low-resolution AOGCMs, Journal of Climate, 34, 2017-2035, 2021.

Schrag, D. P.: Effects of diagenesis on the isotopic record of late Paleogene tropical sea surface temperatures, Chemical Geology, 161, 215-224, 10.1016/s0009-2541(99)00088-1, 1999.

Schrag, D. P., Hampt, G., and Murray, D. W.: Pore fluid constraints on the temperature and oxygen isotopic composition of the glacial ocean, Science, 272, 1930-1932, 1996.

Schrag, D. P., Adkins, J. F., McIntyre, K., Alexander, J. L., Hodell, D. A., Charles, C. D., and McManus, J. F.: The oxygen isotopic composition of seawater during the Last Glacial Maximum, Quaternary Science Reviews, 21, 331-342, 2002.

https://doi.org/10.5194/egusphere-2024-3010
Preprint. Discussion started: 27 September 2024

Seltzer, A. M., Davidson, P.W., Shackleton, S.A., Nicholson, D.P., Khatiwala, S.: Global ocean cooling of 2.3°C during the Last Glacial Maximum, Geophysical Research Letters, 51, e2024GL108866, 2024.

Shackleton, S., Seltzer, A., Baggenstos, D., and Lisiecki, L.: Benthic δ18O records Earth's energy imbalance, Nature Geoscience, 16, 797-802, 2023.

Shackleton, S., Bereiter, B., Baggenstos, D., Bauska, T. K., Brook, E. J., Marcott, S. A., and Severinghaus, J. P.: Is the noble gas-based rate of ocean warming during the Younger Dryas overestimated?, Geophysical Research Letters, 46, 5928-5936, 10.1029/2019gl082971, 2019.

Shackleton, S., Menking, J. A., Brook, E., Buizert, C., Dyonisius, M. N., Petrenko, V. V., Baggenstos, D., and Severinghaus, J. P.: Evolution of mean ocean temperature in Marine Isotope Stage 4, Clim. Past, 17, 2273-2289, 10.5194/cp-17-2273-2021, 2021.

Shackleton, S., Baggenstos, D., Menking, J. A., Dyonisius, M. N., Bereiter, B., Bauska, T. K., Rhodes, R. H., Brook, E. J., Petrenko, V. V., McConnell, J. R., Kellerhals, T., Haberli, M., Schmitt, J., Fischer, H., and Severinghaus, J. P.: Global ocean heat content in the Last Interglacial, Nature Geoscience, 13, 77-81, 10.1038/s41561-019-0498-0, 2020.

Shakun, J. D., Lea, D. W., Lisiecki, L. E., and Raymo, M. E.: An 800-kyr record of global surface ocean delta O-18 and implications for ice volume-temperature coupling, Earth and Planetary Science Letters, 426, 58-68, 10.1016/j.epsl.2015.05.042, 2015.

Shakun, J. D., Clark, P. U., He, F., Marcott, S. A., Mix, A. C., Liu, Z. Y., Otto-Bliesner, B., Schmittner, A., and Bard, E.: Global warming preceded by increasing carbon dioxide concentrations during the last deglaciation, Nature, 484, 49-55, 2012.

Siddall, M., Honisch, B., Waelbroeck, C., and Huybers, P.: Changes in deep Pacific temperature during the mid-Pleistocene transition and Quaternary, Quaternary Science Reviews, 29, 170-181, 10.1016/j.quascirev.2009.05.011, 2010.

Sosdian, S. and Rosenthal, Y.: Deep-sea temperature and ice volume changes across the Pliocene-Pleistocene climate transitions, Science, 325, 306-310, 10.1126/science.1169938, 2009.

Sosdian, S. and Rosenthal, Y.: Response to Comment on "Deep-sea temperature and ice volume changes across the Pliocene-Pleistocene climate transitions", Science, 328, 10.1126/science.1186768, 2010.

Sosdian, S. M., Rosenthal, Y., and Toggweiler, J. R.: Deep Atlantic carbonate ion and $CaCO_3$ compensation during the Ice Ages, Paleoceanography and Paleoclimatology, 33, 546-562, 10.1029/2017pa003312, 2018.

Spero, H. J., Bijma, J., Lea, D. W., and Bemis, B. E.: Effect of seawater carbonate concentration on foraminiferal carbon and oxygen isotopes, Nature, 390, 497-500, 1997.

Spratt, R. M. and Lisiecki, L. E.: A Late Pleistocene sea level stack, Climate of the Past, 12, 1079-1092, 10.5194/cp-12-1079-2016, 2016.

Tierney, J. E., Zhu, J., King, J., Malevich, S. B., Hakim, G. J., and Poulsen, C. J.: Glacial cooling and climate sensitivity revisited, Nature, 584, 569-573, 10.1038/s41586-020-2617-x, 2020.

Uemura, R., Motoyama, H., Masson-Delmotte, V., Jouzel, J., Kawamura, K., Goto-Azuma, K., Fujita, S., Kuramoto, T., Hirabayashi, M., Miyake, T., Ohno, H., Fujita, K., Abe-Ouchi, A., Iizuka, Y., Horikawa, S., Igarashi, M., Suzuki, K., Suzuki, T., and Fujii, Y.: Asynchrony between Antarctic temperature and CO_2 associated with obliquity over the past 720,000 years, Nature Communications, 9, 961, 10.1038/s41467-018-03328-3, 2018.

von Schuckmann, K., Minière, A., Gues, F., Cuesta-Valero, F. J., Kirchengast, G., Adusumilli, S., Straneo, F., Ablain, M., Allan, R. P., Barker, P. M., Beltrami, H., Blazquez, A., Boyer, T., Cheng, L., Church, J., Desbruyeres, D., Dolman, H., Domingues, C. M., García-García, A., Giglio, D., Gilson, J. E., Gorfer, M., Haimberger, L., Hakuba, M. Z., Hendricks, S., Hosoda, S., Johnson, G. C., Killick, R., King, B., Kolodziejczyk, N., Korosov, A., Krinner, G., Kuusela, M., Landerer, F. W., Langer, M., Lavergne, T., Lawrence, I., Li, Y., Lyman, J., Marti, F., Marzeion, B., Mayer, M., MacDougall, A. H., McDougall, T., Monselesan, D. P., Nitzbon, J., Otosaka, I., Peng, J., Purkey, S., Roemmich, D., Sato, K., Sato, K., Savita, A., Schweiger, A., Shepherd, A., Seneviratne, S. I., Simons, L., Slater, D. A., Slater, T., Steiner, A. K., Suga, T., Szekely, T., Thiery, W., Timmermans, M. L., Vanderkelen, I., Wjiffels, S. E., Wu, T., and Zemp, M.: Heat stored in the Earth system 1960–2020: where does the energy go?, Earth Syst. Sci. Data, 15, 1675-1709, 10.5194/essd-15-1675-2023, 2023.

Waelbroeck, C., Labeyrie, L., Michel, E., Duplessy, J. C., McManus, J. F., Lambeck, K., Balbon, E., and Labracherie, M.: Sea-level and deep water temperature changes derived from benthic foraminifera isotopic records, Quaternary Science Reviews, 21, 295-305, 2002.

Weiffenbach, J. E., Dijkstra, H. A., von der Heydt, A. S., Abe-Ouchi, A., Chan, W. L., Chandan, D., Feng, R., Haywood, A. M., Hunter, S. J., Li, X., Otto-Bliesner, B. L., Peltier, W. R., Stepanek, C., Tan, N., Tindall, J. C., and Zhang, Z.: Highly stratified mid-Pliocene Southern Ocean in PlioMIP2, Clim. Past, 20, 1067-1086, 10.5194/cp-20-1067-2024, 2024.

https://doi.org/10.5194/egusphere-2024-3010
Preprint. Discussion started: 27 September 2024

Westerhold, T., Marwan, N., Drury, A. J., Liebrand, D., Agnini, C., Anagnostou, E., Barnet, J. S. K., Bohaty, S. M., De Vleeschouwer, D., Florindo, F., Frederichs, T., Hodell, D. A., Holbourn, A. E., Kroon, D., Lauretano, V., Littler, K., Lourens, L. J., Lyle, M., Palike, H., Rohl, U., Tian, J., Wilkens, R. H., Wilson, P. A., and Zachos, J. C.: An astronomically dated record of Earth's climate and its predictability over the last 66 million years, Science, 369, 1383-1387, 10.1126/science.aba6853, 2020.

Winnick, M. J. and Caves, J. K.: Oxygen isotope mass-balance constraints on Pliocene sea level and East Antarctic Ice Sheet stability, Geology, 43, 879-882, 10.1130/g36999.1, 2015.

Woodard, S. C., Rosenthal, Y., Miller, K. G., Wright, J. D., Chiu, B. K., and Lawrence, K. T.: Antarctic role in Northern Hemisphere glaciation, Science, 346, 847-851, 10.1126/science.1255586, 2014.

Yu, J. M. and Broecker, W. S.: Comment on "Deep-sea temperature and ice volume changes across the Pliocene-Pleistocene climate transitions", Science, 328, 10.1126/science.1186544, 2010.

Zachos, J., Pagani, M., Sloan, L., Thomas, E., and Billups, K.: Trends, rhythms, and aberrations in global climate 65 Ma to present, Science, 292, 686-693, DOI 10.1126/science.1059412, 2001.

Zanna, L., Khatiwala, S., Gregory, J. M., Ison, J., and Heimbach, P.: Global reconstruction of historical ocean heat storage and transport, Proceedings of the National Academy of Sciences of the United States of America, 116, 1126-1131, 10.1073/pnas.1808838115, 2019.

Zeebe, R. E.: An explanation of the effect of seawater carbonate concentration on foraminiferal oxygen isotopes, Geochimica et Cosmochimica Acta, 63, 2001-2007, 10.1016/s0016-7037(99)00091-5, 1999.

Zhou, S., Meijers, A. J. S., Meredith, M. P., Abrahamsen, E. P., Holland, P. R., Silvano, A., Sallée, J. B., and Østerhus, S.: Slowdown of Antarctic bottom water export driven by climatic wind and sea-ice change, Nature Climate Change, 13701-709, 2023.

Zhu, C., Sanchez, S., Liu, Z., Clark, P. U., He, C., Wan, L., Lu, J., Zhu, C., Li, L., Zhang, S., and Cheng, L.: Enhanced ocean heat storage efficiency during the last deglaciation, Science Advances, in press, 2024.

Zhu, C. Y., Liu, Z. Y., Zhang, S. Q., and Wu, L. X.: Global oceanic overturning circulation forced by the competition between greenhouse gases and continental ice Sheets during the last deglaciation, Journal of Climate, 34, 7555-7570, 10.1175/jcli-d-21-0125.1, 2021.